

# On the relevance of fatigue in the risk of failure of structural elements exposed to bottom wave slamming

Romain Hascoët<sup>a,\*</sup>, Nicolas Jacques<sup>a</sup>

<sup>a</sup>ENSTA Bretagne, CNRS UMR 6027, IRDL, 2 rue François Verny, 29806 Brest Cedex 9, France

---

## Abstract

This study aims to investigate whether the fatigue damage induced by bottom wave slamming is a failure mode, important to consider when sizing a marine structural element. The shape and structural arrangement of the body exposed to water-wave slamming are considered to be such that the rise time of wave-impact hydrodynamic loads,  $t_{\text{on}}$ , is short compared to the vibratory response timescale,  $t_{\text{vib}}$ , of the structure,  $t_{\text{on}} \ll t_{\text{vib}}$ . Without further specification of the details of the body, two asymptotic structural response regimes are considered: (i) a first regime where the typical wave impact duration,  $t_{\text{imp}}$ , is much shorter than the vibratory response timescale,  $t_{\text{imp}} \ll t_{\text{vib}}$ ; (ii) a second opposite regime where  $t_{\text{imp}} \gg t_{\text{vib}}$ . In the first regime, fatigue is found to be the dominant failure mechanism, and accounting for the risk of failure due to fatigue damage yields design constraints which are significantly more conservative than the constraints obtained from the risk of ultimate strength exceedance. In the second regime, a detailed modeling of the risk of failure poses various challenges.

*Keywords:* water wave, slamming, fatigue, risk of failure, sea state, marine structure

---

## 1. Introduction

The aim of the present paper is to investigate whether fatigue damage can be a failure mode relevant to the design of a marine structural element exposed to bottom wave slamming. The exposed body may be located either above or below the mean sea surface, a slamming event corresponding to the body crossing the sea free-surface, into the water domain. The originality of this study lies in the consideration of bottom wave slamming as a dominant contribution to fatigue damage. This contrasts, for instance, with the fatigue of ship hull girders in waves (see [1, 2] for recent reviews), where slamming is only a secondary source of stress excitation through the whipping mechanism, although it may contribute to a substantial proportion of the cumulated fatigue damage (see, e.g., [3, 4]). The structural element exposed to bottom wave slamming may be, for example, a fin stabilizer on a ship, a tubular element on an offshore platform, or a diving plane on a surfaced submarine. Within this context, the vertical component of the fluid at impact may be considered as the main variable relevant to slamming loads.

*A priori*, a precise modeling of the body structure's risk of failure requires to consider two possible failure modes:

---

\*Corresponding author

Email address: [romain.hascoet@ensta-bretagne.fr](mailto:romain.hascoet@ensta-bretagne.fr) (Romain Hascoët)

- Failure due to stress locally exceeding a specific threshold. The considered threshold is usually the ultimate tensile strength (shortened hereinafter to “ultimate strength”) or the yield strength of the material. The choice between the ultimate and yield strengths depends on whether the occurrence of local plastic deformation is tolerable. When the structural element is designed for a low probability of failure, this failure mode relates to extreme events (i.e. extreme wave impacts) which have a low probability of occurrence over the considered exposure time.
- Failure due to fatigue damage. Fatigue damage will typically be built up by a (very) high number of impacts, cumulated over the exposure time.

One of the main difficulties encountered in modeling the first failure mode is that it requires to apprehend rare and extreme events. This poses challenges in two regards. Firstly, it requires the modeling of the probability of occurrence of extreme environmental conditions: in the present context, extreme waves, which are themselves generated by extreme sea states. Second, the response of the system to these extreme conditions need to be estimated, with the substantial challenge posed by the fact that the kinematics of extreme waves remain uncertain.

The second failure mode (fatigue damage) may be less challenging in terms of excitation and response modeling, as the bulk of the damage may be built up by a class of events which are not particularly rare and extreme. For such a class of events, in situ or lab measurements may be “readily” accessible, while modeling is less complicated and less subject to uncertainties. However, to properly model this second failure mode, one challenge lies in the fact that the long-term fatigue damage is due to the accumulation of a large number of random events (here wave impacts), whose underlying probability distribution (here related to the properties of the encountered sea states) is also random. In this respect, this makes ‘risk-based’ analyses (i.e., the sizing of the marine structure for a given probability of failure) more involved than for the first failure mode.

The aim of this paper is to investigate the relative importance of these two failure modes, when designing a structural element with respect to the risk induced by bottom wave slamming. The configuration is assumed to be such that the structural element experiences a very large number of wave impacts over the exposure duration; the case where the risk of wave impact occurrence is small over the exposure time is not addressed in this study. The latter situation would typically occur when the elevation of the exposed body (vertical position of the body relative to the still water level) is significantly larger than the typical significant wave height encountered in the geographic zone under consideration (see, e.g., [5, 6]). The present study also intends to identify the dominant classes of sea states and wave impacts, which constitute most of the risk. It attempts to remain as generic as possible regarding assumptions, in order to keep findings and conclusions qualitatively general. The structural element exposed to wave slamming is assumed to have a bottom shape and a structure such that the hydrodynamic loads rise sufficiently fast to excite a local vibratory response of the body. The vibratory response is assumed to be dominated by a single structural mode, typically the mode of smallest eigen frequency (e.g. the first bending mode of an elongated tubular element). This dominant vibratory mode is assumed to be responsible for most of the fatigue damage. However, if this assumption were to be relaxed – i.e. if fatigue damage were due to the superposition of multiple modes, with no single mode being dominant – the qualitative findings of the present work are expected to remain valid.

The framework considered in the present study is further detailed in Section 2. It covers the assumptions made regarding the structural stress response following wave impact (§2.1) and the resulting fatigue damage (§2.2). It also covers the assumptions related to the modeling of sea

state occurrence (§2.3), and impact occurrence in a given sea state (§2.4). Section 3 introduces the various case studies which are considered for investigation and discussion. It gives the specifications of the considered case studies (§3.1), and briefly describe the numerical methods used to investigate these case studies (§3.2). In Section 4, the evolution of the failure probability as a function of a structural sizing factor (which sets the magnitude of the stress responses) is considered. The effect of a change in various parameters is investigated in §4.1-4.2. The relative weights of fatigue damage and ultimate strength limit in the risk of failure is addressed in §4.3. The dominant classes of sea states and wave impacts responsible for the risk of failure are specifically investigated in Section 5. The paper ends with a discussion in Section 6, followed by a conclusion in Section 7.

## 2. Framework and Assumptions

### 2.1. Structural response to wave impacts: three asymptotic regimes

During a hydrodynamic impact, the transient loads will lead to the vibratory excitation of the body structure, on condition that the loads evolve sufficiently fast compared with the structure's characteristic response time (see, e.g., [7, 8] for a review on slamming and the resulting hydroelastic response). This condition will be more readily fulfilled for bodies with blunt shapes (e.g. the flat-bottom hull of a ship; tubular elements on an offshore platform; diving planes on a surfaced submarine), for which the rise of hydrodynamic loads at the beginning of the impact can be very short. When considering a structural detail inside the body, the vibratory response will translate into a succession of stress cycles, which may induce fatigue damage. For the sake of simplicity, a single structural mode is assumed to dominate the vibratory response, as well as the resulting fatigue damage. Then, the condition for a vibratory response can be written as:

$$t_{\text{vib}} \gg t_{\text{on}}, \quad (1)$$

where  $t_{\text{on}}$  is the characteristic time of the hydrodynamic load onset, and  $t_{\text{vib}}$  is the eigen period of the dominant mode (i.e., the characteristic time of the vibratory response). Then, if condition (1) is fulfilled, two regimes can be further distinguished depending on how  $t_{\text{vib}}$  compares with the overall impact duration,  $t_{\text{imp}}$ . Hence, as illustrated in Fig. 1, three different asymptotic stress-response regimes may be distinguished:

1.  $t_{\text{vib}} \ll t_{\text{on}}$ : no significant vibratory response is excited; the stress response is close to be quasistatic.
2.  $t_{\text{on}} \ll t_{\text{vib}} \ll t_{\text{imp}}$ : in this regime, the first cycles of the oscillatory structural response develop, while the hydrodynamic load has not yet decayed much. During this early stage, the excitation load may be approximated by a Heavyside step function. Then, the hydrodynamic load evolves slowly with respect to the vibratory timescale, and the oscillatory component of the response monotonically decays, with no further excitation.
3.  $t_{\text{vib}} \gg t_{\text{imp}}$ : in this regime, the response time of the structure is long compared to the excitation duration. From a structural response perspective, the excitation load can be considered as an impulse; i.e. it may be modeled as a Dirac delta function.

These different regimes are not specific to hydroelastic slamming, but pertain to any elastic system submitted to a transient load. In cases where the body shape is not blunt (e.g. a wedge-shaped body), the rise time of hydrodynamic loads may be comparable to the impact duration, i.e.  $t_{\text{on}} \simeq$

$t_{\text{imp}}$ . In such a situation, the second asymptotic regime listed above ( $t_{\text{on}} \ll t_{\text{vib}} \ll t_{\text{imp}}$ ) does not exist. In the context of hydroelastic slamming, regimes 1 and 3 have been well identified, for instance, in experiments and calculations of the water entry of a wedge [9]. Regime 2 has been identified, for instance, in a recent experimental study of a hydrofoil exposed to water waves [10].

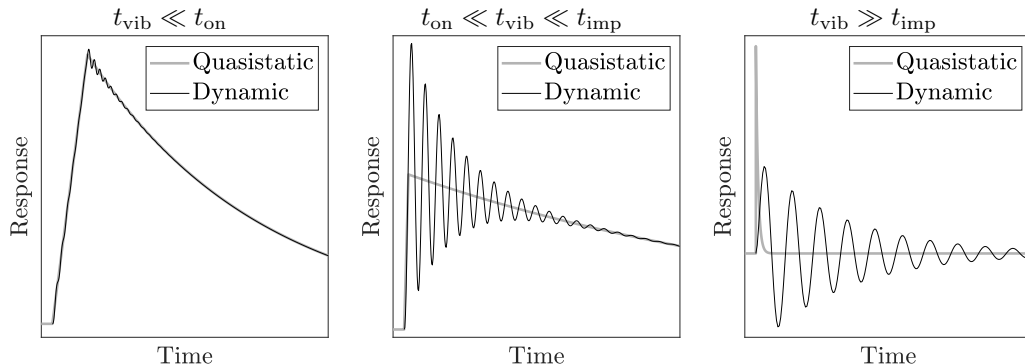


Figure 1: Illustration of the different stress-response regimes considered in the present study. The vibratory mode with the largest eigen period is assumed to dominate the stress response of the structural detail under consideration. Across the three panels the quasistatic response (i.e. assuming static equilibrium at each time) is shown as a grey line. Left: when the vibratory response period,  $t_{\text{vib}}$ , is much shorter than both the onset time and duration of the impact load,  $t_{\text{on}}$  and  $t_{\text{imp}}$  respectively, the stress response is close to being quasistatic. Middle: when the vibratory response period is much longer than the load onset, but much smaller than the load duration,  $t_{\text{on}} \ll t_{\text{vib}} \ll t_{\text{imp}}$ , the amplitude of the first cycle is comparable to the magnitude of the quasistatic counterpart. Right: when the vibratory response timescale is much longer than the load timescale,  $t_{\text{vib}} \gg t_{\text{imp}}$ , the amplitude of the first cycle is approximately proportional to the quasistatic impulse (i.e., the time-integral of the quasistatic response).

It should be noted that the hydroelastic coupling needs to be considered when evaluating  $t_{\text{vib}}$  (due to added-inertia effects). Also, if the coupling is strong, there may be significant feedback from the structural response on the slamming-induced load; see, e.g., [11, 12, 13, 14, 15] for a sample of studies addressing hydroelastic slamming. Besides, ventilation and cavitation phenomena may further complicate the situation (see, e.g., [16] for a recent study on the subject). However, hydroelasticity details are not expected to affect the broad features of the three stress-response regimes depicted in Fig. 1.

Below, in Sections 3-4-5, only the vibratory stress-response regimes (i.e., regimes 2. and 3., as listed above) are investigated with respect to the fatigue-related risk. The case of the quasistatic regime is discussed in section 6.3. Following the initial vibratory excitation, if no further fast variation occurs in the hydrodynamic load, the oscillations are expected to decay monotonically.<sup>1</sup> For the sake of simplicity, the related damping ratio,  $\zeta$ , is assumed to be constant and much smaller than unity,  $\zeta \ll 1$ . According to these assumptions, the stress response of a structural detail, induced by a wave impact, can be modeled as a succession of cycles with decaying amplitudes that

<sup>1</sup> A second excitation episode may be experienced for bodies which are prone to secondary impacts (see, e.g., [17, 18, 19]).

can be approximated as follows:

$$\frac{s^{(k)}}{s^{(1)}} \simeq \exp\{-2\pi\zeta(k-1)\}, \quad (2)$$

where  $s^{(1)}$  and  $s^{(k)}$  are respectively the amplitudes of the 1<sup>st</sup> and  $k^{\text{th}}$  cycles. The structural vibratory response is assumed to have time to mostly dampen between two successive wave impacts.

According to Eq. (2), the sequence of stress-cycle amplitudes, triggered by a wave impact, is entirely determined by the amplitude of the first cycle,  $s^{(1)}$ . In the present study, the magnitude of the stress response is assumed to depend solely on the vertical component of the fluid velocity.<sup>2</sup> The slamming hydrodynamic force and impulse (i.e., the time-integration of the hydrodynamic force) respectively respond quadratically and linearly to the impact velocity. The linear dependence of the impulse on the impact velocity derives from the fact that the characteristic impact duration,  $t_{\text{imp}}$ , is inversely proportional to the impact velocity. Then, if the stress responds linearly to the load magnitude (linear elasticity), the first-cycle amplitude may be modeled as follows:

$$s^{(1)} = S_* \left( \frac{w}{1 \text{ m/s}} \right)^r, \quad (3)$$

where  $w$  is the vertical component of the fluid velocity at impact, and  $S_*$  is a stress normalization factor, which depends on the sizing of the structural element under consideration. The response exponent,  $r$ , depends on the asymptotic vibratory regime considered:

- $t_{\text{vib}} \gg t_{\text{imp}}$ : the magnitude of the stress response is proportional to the hydrodynamic force impulse and is therefore also proportional to the fluid velocity, leading to  $r = 1$ .
- $t_{\text{vib}} \ll t_{\text{imp}}$ : the magnitude of the stress response is proportional to the peak value of the hydrodynamic force, and therefore to the squared value of the fluid velocity, leading to  $r = 2$ .

The intermediate stress-response regimes, where  $t_{\text{vib}} \simeq t_{\text{imp}}$ , or  $t_{\text{vib}} \simeq t_{\text{on}}$ , are not considered in the present study, as they do not lend themselves to simplified modeling. The quantitative investigation of such configurations would require to further specify the shape of the body and its structural arrangement, together with a more advanced hydroelasticity model. Such an undertaking lies beyond the scope of the present study.

## 2.2. Fatigue damage

This subsection describes how fatigue damage is modeled. In §2.2.1 the assumed  $SN$  curve pattern is introduced. In §2.2.2 the recommendation of classification societies regarding the modeling of the  $SN$  curve randomness are briefly reviewed. In relation to this latter point, the following paragraph, §2.2.3, describes the alternative assumptions to be tested in the present study. Finally, §2.2.4 briefly discusses the failure criteria used in the present work.

---

<sup>2</sup>For bottom wave slamming, the vertical component of the fluid velocity, at impact, is usually considered to be the most decisive variable when estimating the resulting slamming loads (see, e.g., [20, 21, 22, 23, 24]). Depending on the shape of the slamming-exposed body, and the desired degree of accuracy, it may be important to include additional kinematic variables – for instance, the free-surface slope, the horizontal fluid velocity, or the fluid acceleration – as input of the considered slamming model (see, e.g., [25, 26, 27, 28, 29]).

### 2.2.1. *SN curve pattern*

A variety of empirical laws has been proposed to model the fatigue stress – life relations of metals (see [30, 31] for reviews on the subject). These relations are also referred to as *SN* curves, where  $N$  is the number of cycles to failure, for a given stress-cycle amplitude (or range),  $S$ . The metal considered in the present marine context is steel, as it is widely used in the naval & offshore industry. When fatigue damage occurs in the high cycle regime ( $10^7 > N > 10^4$ ) and in the very high cycle regime ( $N > 10^7$ ), classification societies have proposed guidelines regarding the *SN* curve patterns, which can be used for the fatigue assessment of ship structures (see, e.g., [32, 33, 34]). These *SN* curve patterns are composed of two power-law branches:

- A high cycle power-law branch,  $S \propto N^{-1/m}$ , valid for  $10^7 > N > 10^4$ . Depending on the geometry and surface finishing of the structural detail, classification societies recommend using an index  $m$  ranging from 3 to 4. In this study,  $m = 3$  is adopted for the illustrative examples to be investigated below.
- A very high cycle power-law branch,  $S \propto N^{-1/(m+\Delta m)}$ , starting from  $N = 10^7$ , with  $\Delta m = 2$  being the value recommended by classification societies. The two branches are connected at  $N = 10^7$ . In this study, in order to limit the number of cycles that need to be considered, the very-high cycle branch is truncated above  $N = 10^{12}$ ; i.e., an endurance limit is set to  $S(N = 10^{12})$ . This latter assumption is adopted for computation convenience; the precise choice of the endurance limit modeling has no effect on the qualitative findings of the present study.

Through the illustrative examples provided in Sections 4-5, it will be shown that this *SN* curve pattern – which is limited to  $N > 10^4$  – is indeed sufficient to estimate the risk of failure, in cases where the structural stress responds linearly to the impact velocity ( $t_{\text{vib}} \gg t_{\text{imp}}$ ). However, in the opposite regime, in which the structural stress responds quadratically to the impact velocity ( $t_{\text{vib}} \ll t_{\text{imp}}$ ), rare and extreme events present a larger weight (relative to “milder” and more frequent events) in terms of induced damage. Then, the evaluation of the risk of failure requires that two additional aspects are accounted for: (i) the damage contribution of stress cycles working within the low cycle regime (fatigue regime where plastic deformations become significant); (ii) the possibility that a single extreme event leads to failure through the exceedance of ultimate strength. In order to cover these two aspects in the present study, the *SN* curve pattern proposed by classification societies has been extended towards the low cycle region ( $N < 10^4$ ) by a third power-law branch. To decide on how to parametrize this third branch, the ultimate strength of the material,  $S_u$ , has been considered to be a good proxy for the stress cycle amplitude at  $N = 1$ :  $S(N = 1) \equiv S_0 \simeq S_u$ .<sup>3</sup> This consideration has led to the choice of  $S_0 = 2 \times S(N = 10^4)$ . Indeed, for the normalization of the *SN* curve patterns, classification societies recommend using  $S(N = 10^4) \simeq 200 - 300$  MPa, which leads to  $S_u \simeq 2 \times S(N = 10^4) \simeq 400 - 600$  MPa. This latter range is consistent with the ultimate strengths reported for steels commonly used in the marine industry (see, e.g., [35, 36, 37]). This set of assumptions leads to the *SN* curve pattern shown in the left panel of Fig. 2.

The effects of mean stress on fatigue life is not considered in this study. On the one hand, the

---

<sup>3</sup>An alternative option could have been to map  $S_u$  to  $S(N = 1/2)$  or  $S(N = 1/4)$ ;  $N = 1/2$  and  $N = 1/4$  respectively corresponding to a half-cycle and a single monotonic tensile ramp. The precise choice is unimportant in the present study.

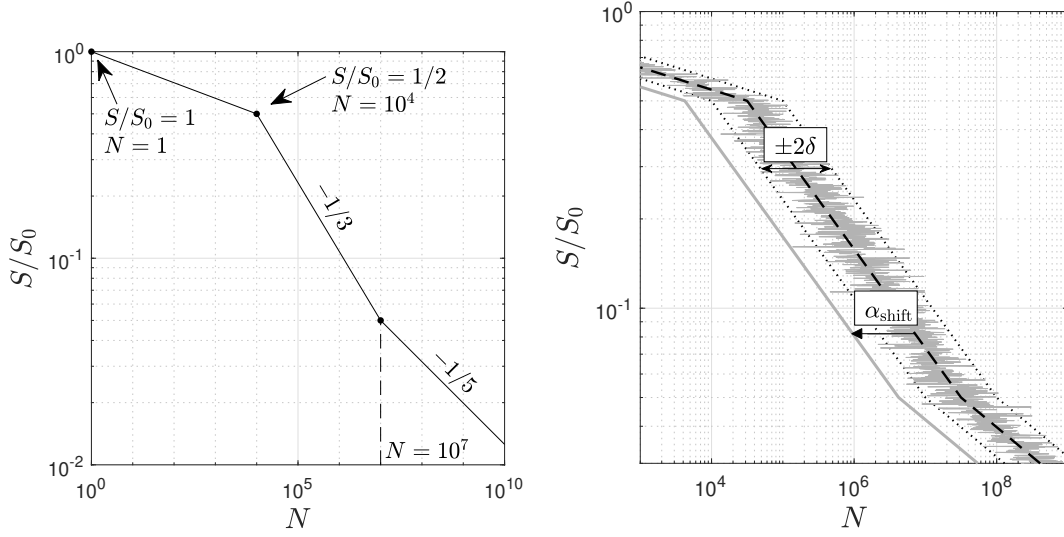


Figure 2: *Left*:  $SN$  curve pattern used in this study. The different constraints which define this  $SN$  curve are annotated: (i) the stress amplitude at  $N = 1$ ,  $S_0 \equiv S(N = 1)$ , is used as a normalization factor of the proposed  $SN$  curve pattern.  $S_0$  is expected to be close to the ultimate strength of the material; (ii) the stress level at the end of the low cycle branch is set to  $S = S_0/2$  at  $N = 10^4$ . The transition stress level,  $S_0/2$ , can be considered as a proxy for the yield strength; (iii) the power law index of the high cycle branch is equal to  $-1/3$ ; (iv) the very high cycle branch starts at  $N = 10^7$  and has a power law index equal to  $-1/5$ . *Right*:  $SN$  curve randomness. In the illustration, the median  $SN$  curve is shown as a dashed line. The noisy grey curve illustrates the case where the randomness is modeled through option 2 (see text). The solid grey curve illustrates the case where the randomness is modeled through a random shift factor,  $\alpha_{\text{shift}}$  (option 1). The dotted lines show the  $\pm 2\delta$  band. The “ $-2\delta$ ” curve (i.e., the dotted line on the left of the median  $SN$  curve) matches the curve pattern shown on the left panel.

mean stresses of cycles are expected to be close to zero (full stress reversal) in the linear stress-response regime, where the load excitation can be considered as an impulse (see right panel in Fig. 1). On the other hand, in the quadratic response regime (see middle panel in Fig. 1), cycle means are expected to be comparable, in magnitude, to cycle amplitudes. In this latter regime, an accurate estimate of fatigue damage would require the effect of the mean stresses to be accounted for, for instance, by using a Goodman-type relation or a Gerber-type relation (see, e.g., [30, 31]). A short discussion of the anticipated effect of cycle mean stresses is reported in Appendix A.

### 2.2.2. $SN$ curve randomness: recommendations from classification societies

Fatigue tests show significant dispersion in the results obtained from experiments repeated in the same conditions; for a given fixed stress amplitude, the observed number of cycles to failure can vary greatly from one trial to another. As stated by Stephens et al. (2000) [31] this variability may be due to “inherent material variability, variations in heat treatment and manufacturing, variations in specimen or component geometry, and variations from differences in the testing conditions”. Usually, for a given stress amplitude, the dispersion of observed cycle numbers to failure can be satisfactorily fitted by using a log-normal distribution or a Weibull distribution.

For a given failure probability,  $P_\epsilon$ , classification societies propose (e.g. [32, 33, 34]) to size a marine structure against fatigue by using a deterministic  $SN$  relation,  $N_{P_\epsilon}(S)$ , which is defined as

follows. For a given stress amplitude,  $S$ , the realized random number of cycles to failure,  $n_{|S}$ , has a probability  $P_\varepsilon$  of being lower than  $N_{P_\varepsilon}(S)$ , i.e.,  $P[n_{|S} < N_{P_\varepsilon}(S)] = P_\varepsilon$ . Then, the structure design is considered to pass the fatigue constraint if the *mean* long-term distribution of stress amplitudes, transferred through the design  $SN$  curve, gives a cumulated damage smaller than one (Miner's rule is assumed). Hence, in this approach only the randomness of the  $SN$  curve is considered. The effect of the randomness of wave forcing is assumed to be largely suppressed by the large number of cumulated solicitations. In the documentation issued by classification societies, the reported  $SN$  curve patterns,  $N_{cl}(S)$ , are given for a failure probability  $P_\varepsilon = 0.023$ , which translates as:

$$P[n_{|S} < N_{cl}(S)] = 0.023. \quad (4)$$

Under the assumption that  $n_{|S}$  follows a log-normal distribution, this corresponds to  $\ln(N_{cl}(S))$  being two standard deviations below the mean of  $\ln(n_{|S})$ :

$$\ln(N_{cl}(S)) \simeq E[\ln(n_{|S})] - 2\delta, \quad (5)$$

where  $\delta$  is the standard deviation of  $\ln(n_{|S})$ . In principle,  $\delta$  may depend on the stress amplitude,  $S$ . When there is insufficient experimental data to estimate the standard deviation of  $\ln(n_{|S})$ , Det Norske Veritas [33] and Bureau Vertitas [32] recommend using constant values, respectively  $\delta_{DNV} = 0.2 \times \ln(10)$  and  $\delta_{BV} = 0.25 \times \ln(10)$ .

### 2.2.3. $SN$ curve randomness: assumption adopted in the present study

In this study, the structural detail under study is linked to an  $SN$  curve,  $n(S)$ , which is random, *a priori*. For a given structural detail specimen, the realized instance of  $SN$  curve is assumed to hold during the whole life of the specimen. Then, the fatigue damage,  $D_{cum}$ , accumulated by the specimen is computed using Miner's rule. Assuming that the stress loading history consists of a collection of  $M$  cycles of amplitudes  $s_1, s_2, \dots, s_M$ , Miner's rule reads:

$$D_{cum} = \sum_{k=1}^M \frac{1}{n(s_k)}. \quad (6)$$

For a given stress amplitude, the statistical properties of  $n_{|S} = n(S)$ , can be estimated by conducting fatigue tests at different constant stress amplitudes, using a different specimen for each test. However, for a realized  $SN$  curve (i.e. for a given specimen) the covariance structure between  $n_{|S_1}$  and  $n_{|S_2}$ , the numbers of cycles to failure at two different stress levels,  $S_1$  and  $S_2$ , is more difficult to probe, as a fatigue test cannot be repeated twice with the same specimen. In the literature, this matter has been investigated by modeling  $n(S)$  as the realization of a stochastic process (see, e.g., [38, 39]). In this regard, two extreme assumptions have been tested in the present study:

1. The  $SN$  curve is randomized through a global shift factor applied to the median  $SN$  curve,  $N(S)$ . In other words, for a given specimen, the knowledge of  $n_{|S}$  at a given stress level fully determines the realized  $SN$  curve. In this study, the logarithm of the random shift factor is assumed to follow a centered normal distribution of standard deviation  $\delta = \delta_{BV}$  (introduced above). This configuration corresponds to the approach proposed by classification societies.
2. The randomness of  $\ln(n(S))$  is modeled as a Gaussian white noise: i.e., for a given specimen, the values of  $\ln(n_{|S_1})$  and  $\ln(n_{|S_2})$ , at two different stress levels  $S_1$  and  $S_2$ , are independent random Gaussian variables. The standard deviation of the white noise is set to  $\delta = \delta_{BV}$ . This approach is used for example in [40, 41].



These two extreme situations are illustrated in the right panel of Fig. 2. Computations have shown that option 1 yields the most conservative constraints in the regime of small failure probabilities (which is usually the regime relevant for the design of a marine system). Therefore, it is the modeling option which has been adopted for the case studies presented below.

The fact that option 1 yields constraints which are more conservative than the ones provided by option 2 – in the regime of small failure probabilities – can be understood as follows. On the one hand, for a given sequence of stress cycles of various amplitudes, the mean fatigue damage does not depend on the covariance structure of the  $SN$  curve. On the other hand, the dispersion of the realized fatigue damage (above and below its mean) will be greater when the  $SN$  curve randomness is modeled through assumption 1, because the damages induced at different stress amplitudes will be positively correlated, while they are uncorrelated under assumption 2. As a result, option 1 leads to longer tails in the distribution of the realized fatigue damage, which translates into sizing constraints being more conservative in the regime of small failure probabilities. The same trend has been found and similarly explained in the previous studies [38, 39], where further details can be found.

#### 2.2.4. Failure criteria and failure mode

The structure is considered to fail due to fatigue if the cumulated damage  $D_{\text{cum}}$  (Eq. 6) exceeds one. As the  $SN$  curve is randomized through a global shift of the  $SN$  curve pattern, the ultimate strength,  $S_u$ , can be formally identified with the stress-cycle amplitude for which the realized  $SN$  curve intersects  $N=1$  (thereby,  $S_u$  is a random variable). Then, two failure modes can be distinguished: (i) failure due to a cumulated fatigue damage exceeding one,  $D_{\text{cum}} > 1$  (with no occurrence of ultimate strength exceedance); and (ii) failure due to the occurrence of a stress cycle which has an amplitude exceeding  $S_u$ .

### 2.3. Modeling of sea state occurrence

The long-term sea state history, to which the marine structure is exposed, is modeled as a sequence of short-term stationary sea states. The randomness of a given stationary sea state is parametrized through its significant wave height,  $H_s$  (see Eq. 12 below), and its average wave period,  $T_z$  (see Eq. 13 below). This subsection introduces the different approaches implemented to simulate the random sequence of encountered sea states, on a given geographical site, over a given exposure duration.

#### 2.3.1. sea state populations

In order to investigate how the sea state population may affect the qualitative features of the results obtained in this study, two different sea state populations have been considered:

- A first sea state population which is the population recommended by classification societies for the North Atlantic region (e.g. [42, 43]). The related joint density function of sea states in the plane  $(H_s, T_z)$ , was derived by applying a conditional modeling approach:

$$P_{\text{cs}}(H_s, T_z) = f_{\text{wbl}}(H_s; \alpha_{\text{cs}}, \beta_{\text{cs}}, \gamma_{\text{cs}}) \cdot f_{\text{logn}}[T_z; \mu_{\text{cs}}(H_s), \sigma_{\text{cs}}^2(H_s)] , \quad (7)$$

where  $f_{\text{wbl}}$  denotes the three-parameter Weibull density function of scale parameter  $\alpha_{\text{cs}}$ , shape parameter  $\beta_{\text{cs}}$ , and position parameter  $\gamma_{\text{cs}}$ , and  $f_{\text{logn}}$  denotes the lognormal density function of parameters  $\mu_{\text{cs}}$  and  $\sigma_{\text{cs}}^2$ . For the North Atlantic region, classification societies recommend using  $\alpha_{\text{cs}} = 3.041$ ,  $\beta_{\text{cs}} = 1.484$ ,  $\gamma_{\text{cs}} = 0.661$ ,  $\mu_{\text{cs}}(H_s) = 0.70 + 1.27 H_s^{0.131}$  and

$\sigma_{cs}(H_s) = 0.1334 + 0.0264 \exp(-0.1906 H_s)$ , where  $H_s$  and  $T_z$  are given in meters and seconds, respectively. This is the parametrization used in the present study.

- A second population derived from 10 years of buoy measurements acquired on a site based in the Gulf of Maine. The dataset was used for a benchmarking exercise designed to compare environmental contour methods [44, 45]; the considered dataset is labelled as “dataset A” in [44]. On this US coastal site, sea states are much less severe (in terms of significant wave height) than in the North Atlantic. The joint distribution of sea states in the plane  $(H_s, T_z)$  has been fitted by implementing the storm resampling method, originally proposed by Mackay and Jonathan (2020) [46]. Appendix B gives a brief summary of the method, along with some elements of validation of the implemented version.

### 2.3.2. Serial dependence of encountered sea states

As illustrative examples will show in Section 4, extreme events (extreme sea states and extreme waves) carry a significant weight in the long-term risk of failure, in the quadratic stress-response regime ( $t_{vib} \ll t_{imp}$ ). Then, to properly reckon the long-term risk of failure, it may be important to account for the serial dependence of successive sea states in a realized time series. Sea states are typically considered as stationary on a one-hour window. On the other hand, storm events usually last from several hours to a few days, thereby producing groups of extreme sea states. In order to test the potential effect of sea state serial dependence on the slamming-induced risk of failure, two different approaches have been implemented in this study:

- For the North Atlantic sea state population, a simplified approach has been used. The successive sea states are assumed to be independent, but two different durations have been tested for the stationarity of sea states: namely, 1hr and 24hr. For practical applications, sea states are usually assumed to be stationary over a duration of typically 1hr. Extending the stationarity window to 24h mimics, in a coarse manner, the effect of serial dependence. For a given exposure time, and a given sea state distribution, the occurrence probability of an extreme sea state decreases as the stationarity window is increased, since the total number of encountered sea states decreases. But if extreme conditions do occur, they last longer. The rendered effect is qualitatively the same as storm events generating groups of extreme sea states.
- For the Gulf of Maine sea state population, the storm resampling method proposed by Mackay and Jonathan (2020) [46], has been implemented. Mackay and Jonathan introduced this approach in the context of the benchmarking exercise mentioned above [44, 45]. The bottom line of this method is to divide the historical time series in adjoining “storm” blocks, which can be considered to be independent. The resulting population of storm blocks is fitted in terms of two auxiliary variables. Then, synthetic sea state sequences are generated by randomly drawing a sequence of auxiliary variables, which are used to resample and rescale observed storm blocks. See Appendix B and [46] for further details.

### 2.4. Modeling of impacts in a given sea state

The vertical fluid velocity at impact is the only variable considered to estimate hydrodynamic slamming loads, and the resulting structural vibratory response (see subsection 2.1). In this study, the linear wave framework is used to model impact-related probabilities. The linear wave theory enables the modeling of the randomness of sea waves through Gaussian processes. The exposed body is assumed to be fixed in the reference frame of the mean flow (i.e. the reference frame where

the mean fluid velocity field of water waves is zero).<sup>4</sup> Besides, if the impacted body is sufficiently small in relation to water wave wavelengths, the body can be reduced to a single material point regarding the risk of slamming event; a slamming event corresponding to the sea surface upcrossing the material point. Within this framework, the free-surface elevation measured at the station of the material point,  $\eta(t)$ , can be modeled as a Gaussian process, whose mean is zero (assuming  $\eta(t)$  is measured from the mean water level) and whose power spectrum identifies with the wave spectrum. The control material point is assumed to be fixed at a given altitude  $z = a$ , with respect to the mean water level. In the linear wave model, the vertical component of the fluid velocity,  $w$ , at the free surface, is equal to the time derivative of the free-surface elevation,  $w = \dot{\eta} = d\eta/dt$ . Using level-crossing theory (see, e.g., [47]), it can be shown that  $w|\eta(t) \uparrow a$ , the vertical velocity given that  $\eta(t)$  upcrosses the altitude  $a$ , follows a Rayleigh distribution, whose probability density function reads

$$f_{w|\eta(t)\uparrow a}(w) = \frac{w}{\sigma_w^2} \exp \left\{ -\frac{w^2}{2\sigma_w^2} \right\}. \quad (8)$$

The mode of the Rayleigh distribution,  $\sigma_w$ , is given by

$$\sigma_w^2 = \int_0^{+\infty} \omega^2 \mathcal{S}(\omega) d\omega, \quad (9)$$

where  $\mathcal{S}$  is the one-sided wave spectrum, and  $\omega$  is the wave angular frequency. The integral of the wave spectrum satisfies

$$\int_0^{+\infty} \mathcal{S}(\omega) d\omega = \sigma_\eta^2, \quad (10)$$

where

$$\sigma_\eta^2 = E[\eta^2], \quad (11)$$

is the variance of the free-surface elevation. The significant wave height of the underlying sea state is defined by

$$\sigma_\eta^2 = \frac{H_s^2}{16}. \quad (12)$$

The average zero-upcrossing period (i.e. the average wave period),  $T_z$ , is related to  $\sigma_\eta$  and  $\sigma_w$  through

$$T_z = 2\pi \frac{\sigma_\eta}{\sigma_w}. \quad (13)$$

Combining Eqs. (12-13),  $\sigma_w$  may be expressed as a function of the sea state characteristics:

$$\sigma_w = \frac{\pi}{2} \frac{H_s}{T_z}. \quad (14)$$

In addition to the distribution of impact velocities (Eq. 8), the frequency of slamming events (i.e. the average frequency of upcrossing events) is also needed to reckon the risk of failure related to

---

<sup>4</sup>If the considered body is submitted to seakeeping motions, the Gaussian framework remains applicable, as long as seakeeping responses are modeled through a linear approach (see, e.g., [28]). Moreover, when a forward motion of the body (or equivalently a mean current) would need to be considered, the Gaussian framework would equally remain applicable (see [29]).

wave slamming. Using Rice's formula [48, 49] together with Eqs. (12-13), the upcrossing frequency can be expressed as

$$\mu_{\uparrow a} = \frac{1}{T_z} \exp\{-8(a/H_s)^2\}. \quad (15)$$

From Eqs. (8-14-15), it appears that both the impact frequency and the distribution of impact velocities, for a given sea state, are fully defined by the specification of  $H_s$  and  $T_z$ .

### 3. Case studies

Adopting the framework introduced in the previous section, the question of whether slamming-induced fatigue can be a dominant failure mode is now addressed. To this end, various case studies have been investigated using numerical simulations. The considered case studies are described in Section 3.1. Section 3.2 briefly presents the numerical setup implemented to simulate the considered case studies.

#### 3.1. Simulated scenarios

The various configurations, considered in this study, have been defined by adopting simple assumptions and by varying key parameters, as follows:

- Long-term exposure duration: the body exposed to wave slamming, is supposed to operate during a given duration,  $d_{lt}$ , in the same geographical region, without interruption. To investigate the effect of the exposure duration, the following durations have been considered:  $d_{lt} = 1; 5; 20$  yr.
- The random encounter of sea states is modeled by following the approaches introduced in §2.3. More specifically, four configurations are considered, as listed in Table 1. In the first configuration, sea states are drawn from the Gulf of Maine region, using the storm resampling method. In the second configuration, sea states are drawn from the same Gulf of Maine population, but sea states are made serially independent. In the last two configurations, the sea states are drawn from the North Atlantic population, assuming that sea states are sequentially independent. In the fourth configuration the assumed stationary duration is  $d_{st} = 1$  hr. In the third configuration, in order to mimic the effect of serial dependence in the encountered sea states, the sea state stationarity duration is set to  $d_{st} = 24$  hr.
- The detailed sizing of the structure is summarized by the stress-response normalization factor  $S_*$  (see Eq. 3). Two different asymptotic vibratory stress-response regimes (linear and quadratic) are considered; see Section 2.1. The damping ratio of vibrations following wave impact (see Eq. 2) is fixed to  $\zeta = 10^{-2}$ .
- It is assumed that the body is fixed in the reference frame of the mean flow, at a given altitude,  $a$ , relative to the mean water level (see Section 2.4). The potential effect of tides on the altitude  $a$  (if the structure is bottom-fixed) is not considered. From Eq. (15), the mean number of impacts, for a single sea state exposure, is given by

$$E[N_{ip}^{(st)}] = \frac{d_{st}}{T_z} \exp\left\{-8\left(\frac{a}{H_s}\right)^2\right\}, \quad (16)$$

which is used to set the number of impacts generated by each encountered sea state. In principle, the number of impacts, generated by a given sea state, should be treated as a random variable. However,  $E[N_{\text{ip}}^{(\text{st})}]$  can be used as a reasonable proxy for  $N_{\text{ip}}^{(\text{st})}$  as long as<sup>5</sup>  $E[N_{\text{ip}}^{(\text{st})}] \gg 1$ . In the present illustrative examples the material point is assumed to be at the mean water level ( $a = 0$ ) for simplicity, which guarantees that  $E[N_{\text{ip}}^{(\text{st})}]$  is indeed much larger than unity for all encountered sea states. Moving the control material point away from the mean water level (i.e., increasing the absolute value of  $a$ ), would decrease  $E[N_{\text{ip}}^{(\text{st})}]$  for a given sea state, and would give a larger weight to sea states with large significant wave heights. The effect of a change in the value of  $a$  is further discussed in §6.4.

- The randomness of the  $SN$  curve is modeled according to approach 1, introduced in §2.2.3.

	Region	$d_{\text{st}}$	Serial dependence
<b>sse-1</b>	Gulf of Maine	1hr	SRM
<b>sse-2</b>	Gulf of Maine	1hr	none
<b>sse-3</b>	North Atlantic	24hr	none
<b>sse-4</b>	North Atlantic	1hr	none

Table 1: This table summarizes the different configurations considered to model the sea states encountered by the marine structure. The first column introduces tags which are used below to refer to the different configurations. The second column indicates the geographical region. The third column specifies the duration over which a sea state is assumed to be stationary. The last column indicates whether the serial dependence of successive sea states is modeled: 'none' indicates that successive sea states are modeled as independent events; 'SRM' refers to the storm resampling method [46].

### 3.2. Numerical methods

Following the previous subsection (3.1), a case study is defined by a choice of long-term exposure time  $d_{\text{lt}}$ , sea state modeling approach,  $SN$  randomness modeling approach, and structural stress-response regime. For each investigated case study, a total number of  $N_{\text{lt}} = 10^4$  realizations of long-term exposure are simulated by using a Monte Carlo method, as follows. First, for each long-term realization, a sequence of encountered sea states, covering the long-term exposure duration  $d_{\text{lt}}$ , is drawn in the plane  $(H_s, T_z)$ . Then, for each sea state, the number of impacts is computed from Eq. (16), and the set of realized impact velocities is drawn from a Rayleigh distribution whose mode is set by Eq. (14). This yields a long-term collection of impacts, from which the long-term collection of stress cycles can be derived by using Eqs. (2-3), up to a factor  $S_*$  (representative of the structure sizing). For numerical efficiency, the realized collections of stress-cycle amplitudes are reduced into histograms. Then, each long-term histogram of stress-cycle amplitudes is paired with a realized  $SN$  curve (i.e., a material sample). Finally, for a given value of  $S_*$ , the long-term fatigue damage is computed by applying Miner's rule (Eq. 6).

---

<sup>5</sup>For instance, a Gaussian sea state with an average wave period  $T_z \simeq 8.2$  s and a JONSWAP spectrum (with a peak enhancement parameter  $\gamma = 3.3$ ), running during 1 hr, has been found (by using Monte Carlo simulations) to produce a number of zero-upcrossings,  $N_{\uparrow 0}$ , which has a standard deviation  $\sigma_{N_{\uparrow 0}} \simeq 8.1 \ll E[N_{\uparrow 0}] \simeq 440$ .

#### 4. Probability of failure

This section focuses on the failure probability,  $P_{\text{fail}}$ , as a function of the structural sizing factor,  $S_*$ . Fig. 3 shows the curve  $P_{\text{fail}}(S_*)$  for different combinations of exposure time  $d_{\text{lt}}$ , sea state modeling, and structural dynamical regime. As expected, for a given configuration,  $P_{\text{fail}}(S_*)$  is an increasing function, from 0 (for  $S_* = 0$  there is no structural excitation, and thereby no damage) to 1 (for  $S_* \rightarrow \infty$ , failure occurs almost surely). Subsections 4.1-4.2, specifically analyze the effects of exposure duration and serial dependence in encountered sea states. Subsection 4.3 addresses the degree of conservativeness of the sizing constraints set by an approach which includes fatigue damage, relative to the constraints set by an approach which only considers the risk of ultimate strength exceedance.

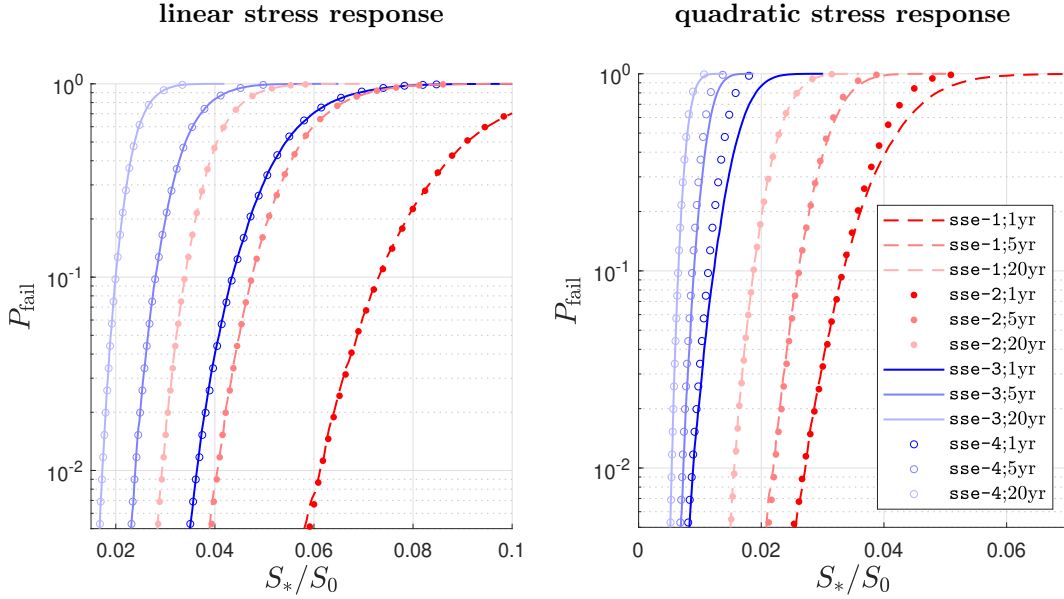


Figure 3: Risk of failure,  $P_{\text{fail}}$ , as a function of the structural sizing factor,  $S_*$ . Results for the linear (resp. quadratic) stress-response regime are shown on left (resp. right) panel. Four different configurations are considered to model encountered sea states, **sse-1**, **sse-2**, **sse-3**, **sse-4**, as listed in Tab. 1, and labelled in the legend of this figure. Gradations of colors (grey in black and white version) are used to differentiate the considered exposure durations. The dots (resp. dashed and solid lines) show results when serial dependence in sea state sequences is neglected (resp. considered). The structural sizing factor  $S_*$  is nondimensionalized by the parameter  $S_0$ , which has been used to normalize the  $SN$  curves (see Fig. 2).

##### 4.1. Effect of exposure time $d_{\text{lt}}$

As expected, and as illustrated by Figs. 3-4, the failure probability increases as the exposure time is increased, other things equal. For a fixed failure probability  $P_{\text{fail}} = P_\varepsilon$ , in the range  $P_\varepsilon < 0.1$ , an increase in the exposure time from  $d_{\text{lt}} = 1$  yr to  $d_{\text{lt}} = 20$  yr, translates into a decrease in the structural sizing factor,  $S_*$ , by a factor ranging from  $\simeq 1.4$  to  $\simeq 2.2$ , depending on the considered configuration.

#### 4.2. Effect of serial dependence in encountered sea states

The consideration of serial dependence in successive encountered sea states affects the predicted failure probability, only in the quadratic dynamical regime,  $r = 2$ . This is illustrated by Fig. 3, where the failure probability,  $P_{\text{fail}}(S_*)$ , is shown for four different sea state modelings. In an initial series of three pairs of curves (each pair corresponding to a different exposure duration), the encountered sea states are drawn as serially independent, from the North Atlantic population, but with different sea state durations,  $d_{\text{st}} = 1$  hr (**sse-4**) and  $d_{\text{st}} = 24$  hr (**sse-3**). The case where  $d_{\text{st}} = 24$  hr intends to roughly mimic the effect of serial dependence (see §2.3.2). In a second series, sea states are from the Gulf of Maine population, either drawn as serially independent (**sse-2**), or made serially dependent through the storm resampling method (**sse-1**).

For both series, the failure probability,  $P_{\text{fail}}$ , is smaller when serial dependence is accounted for. This trend can be explained as follows. For a same population of sea states, the serial dependence will decrease the chance of encountering an extreme sea state over a given exposure duration. However, if one extreme sea state occurs, others are likely to follow, extreme sea states occurring in groups. Besides, in the quadratic stress-response regime, failure scenarios are divided into two distinct classes (see Section 5 for a more detailed analysis of this point): (i) a first class where the damage leading to failure is due to the accumulation of a large number of impacts, generated by a large number of encountered sea states; (ii) a second class where the damage leading to failure is dominated by a single impact, generated by a single extreme sea state. Short-term serial dependence in successive sea states has the effect of grouping extreme sea states, which leads – other things equal – to a decrease in the probability of encountering an extreme sea state over a given duration. If an extreme sea state occurs and leads to failure, it does not matter whether this sea state is followed by other extreme sea states. Therefore, for a given sea state distribution, serial dependence effectively decreases the probability of class (ii) failure occurrences. Conversely, serial dependence does not affect the probability of class (i) failure occurrences. Hence, the net effect of serial dependence is to decrease the total probability of failure.

In the linear stress-response regime, accounting for the serial dependence of encountered sea states is of no significance, as the subpopulation of failures dominated by the encounter of a single extreme sea state is suppressed. This difference is due to the fact that extreme wave impacts are given a larger weight – in terms of induced damage – in the quadratic stress-response regime.

In Fig. 3, right panel, one can also notice that the effect of serial dependence in encountered sea states weakens as  $S_*$  decreases (corresponding to decreasing failure probabilities). Besides, other things equal, the effect of serial dependence also appears to weaken when the exposure time is increased. In essence, these two trends find the same explanation: accounting for serial dependence becomes unimportant when the risk of failure carried by a group of extreme sea states (generated by a single storm) becomes significantly smaller than unity. Indeed, in this regime, the probability of failure induced by a group of consecutive extreme sea states is approximately equal to the sum of individual failure probabilities carried by the same extreme sea states, considered in isolation. Then, to assess  $P_{\text{fail}}$ , it does not matter whether sea states are modeled as serially dependent or independent.

When examining the results shown in Fig. 3, the present case studies – for both considered sea state populations – suggest that accounting for serial dependence of sea states becomes unimportant when  $d_{\text{lt}}/P_{\text{fail}} \gtrsim 50$  yr. From an “rare event” perspective, the ratio  $d_{\text{lt}}/P_{\text{fail}}$  can be interpreted as a return period

$$T_{\text{r}} \simeq d_{\text{lt}}/P_{\text{fail}}, \quad (17)$$

subject to  $P_{\text{fail}} \ll 1$ . The constraint  $T_r \gtrsim 50$  yr defines a region for the parameter space which is usually relevant and sufficient for the design of marine structures. However, it should be noted that the degree of sensitivity to the serial dependence in encountered sea states, depends on the considered sea state population; see Section 5 in [50], for an illustration and a discussion of this matter. In any case, it is worth noting that ignoring the sea state serial dependence in the risk assessment, leads to sizing limits which are conservative with respect to the case where serial dependence is accounted for.

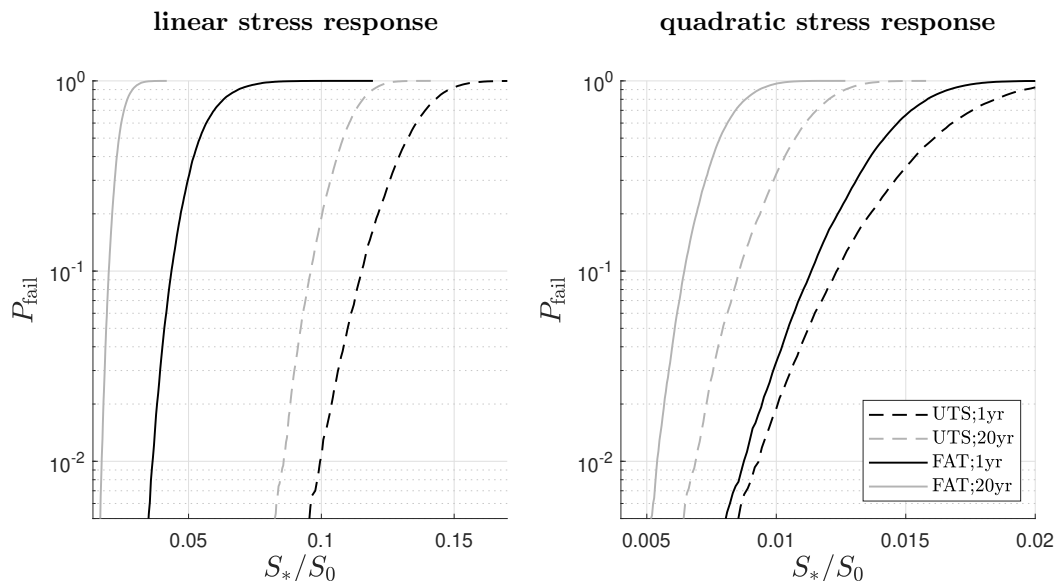


Figure 4: Risk of failure,  $P_{\text{fail}}$ , as a function of the structural sizing factor,  $S_*$ . Comparison of  $P_{\text{fail}}$  estimates when the risk induced by fatigue is accounted for (curves labeled as ‘FAT’ in the legend), or when only the risk of ultimate strength exceedance is considered (curves labeled as ‘UTS’ in the legend). The results for the linear (resp. quadratic) stress-response regime are shown on the left (resp. right) panel. Two different exposure durations are considered:  $d_{\text{lt}} = 1$  yr (black) and  $d_{\text{lt}} = 20$  yr (grey). Sea states are drawn from the North Atlantic population, with a stationarity duration  $d_{\text{st}} = 1$  hr (configuration labelled as ‘sse-4’ in Tab. 1).

#### 4.3. Risk of failure due to ultimate strength exceedance vs fatigue damage

Fig. 4 compares, as a function of  $S_*$ , the probability of failure induced by fatigue damage, with the probability of failure obtained when only the risk of ultimate strength exceedance is considered (fatigue damage is ignored). Below,  $P_{\text{fail}}^{(\text{u})}$  is used to denote the probability of ultimate strength exceedance for a given sizing factor; and  $S_*^{(\text{u})}$  is used to denote the sizing factor corresponding to a given probability of ultimate strength exceedance. As expected, for a given configuration and a given value of  $S_*$ ,  $P_{\text{fail}}^{(\text{u})}$  is smaller than  $P_{\text{fail}}$ , as the risk induced by fatigue is ignored when computing  $P_{\text{fail}}^{(\text{u})}$ . In the case of the linear stress-response regime (left panel of Fig. 4), there is no overlap between the risks related to fatigue damage and to ultimate strength exceedance. Here, “no overlap” means that – as  $S_*$  is decreased (for a given configuration) –  $P_{\text{fail}}^{(\text{u})}$  becomes vanishingly small before  $P_{\text{fail}}$  starts to significantly depart from unity. Hence, in the region of the parameter



space where  $P_{\text{fail}} \lesssim 0.1$  the risk of failure is essentially due to fatigue damage, while the risk of ultimate strength exceedance brings no contribution. Also, for a given probability of failure, the structural sizing factor is noticeably larger (i.e., noticeably less conservative), when the risk due to fatigue damage is ignored. Among the considered configurations, for a small failure probability  $P_\varepsilon \lesssim 0.01$  (region of the parameter space usually relevant for practical applications), the ratio  $S_*^{(u)}(P_\varepsilon)/S_*(P_\varepsilon)$  is in the range  $\simeq 2 - 5$ .

Conversely, in the quadratic stress-response regime, the curves  $P_{\text{fail}}(S_*)$  and  $P_{\text{fail}}^{(u)}(S_*)$  (for a same configuration) get much closer, and there is a significant “overlap” in the risks of failure due to fatigue damage and due to ultimate strength exceedance. For  $P_\varepsilon \lesssim 0.01$ ,  $S_*^{(u)}/S_*$  is in the range  $\simeq 1.05 - 1.5$ , depending on the considered configuration.

## 5. Properties of realizations leading to failure

This section focuses on the identification of the dominant classes of sea states and wave impacts leading to failure. With respect to reliability analysis, the following important question arises: is the damage leading to failure built up by a very large number of rather frequent events, or is it mostly dominated by rather rare and extreme events? Second, with respect to the modeling of wave impacts, a correlating important question relates to the degree of nonlinearity of risk-predominant sea states and waves. These two questions are addressed in terms of sea states in §5.2, and in terms of individual waves in §5.3. Then, subsection 5.4 investigates the relative contributions of the different damage channels (i.e. the different fatigue regimes, along with the ultimate strength exceedance) to the risk of failure.

### 5.1. Considered case study

Below, these different matters are investigated for one specific configuration: encountered sea states are drawn from the sea state population **sse-4** (North Atlantic region with  $d_{\text{st}} = 1$  hr; see Tab. 1), and the exposure duration is set to  $d_{\text{lt}} = 10$  yr. The structural sizing factor  $S_*$  is set to a value such that the probability of failure is  $P_{\text{fail}} = 2.3\%$ , over the exposure duration. Results obtained for the two different vibratory stress-response regimes, linear and quadratic, are compared. It has been checked that the specific choice of the considered configuration is not crucial in the present section; the qualitative features, which will be presented and discussed below, remain when the different parameters are changed.

### 5.2. Dominant class of damaging sea states

Fig. 5 shows the damage cumulation to failure, as a function of the sea state wave steepness,  $\kappa$ . The characteristic wave steepness of a given sea state is defined as

$$\kappa = k_z \frac{H_s}{2}. \quad (18)$$

The wave number  $k_z$  is defined as being related to  $T_z$  through the linear dispersion relation

$$k_z = \frac{1}{g} \left( \frac{2\pi}{T_z} \right)^2, \quad (19)$$

leading to

$$\kappa = \frac{2\pi^2}{g} \frac{H_s}{T_z^2}. \quad (20)$$

In Eq. (19), the water depth is assumed to be infinite. This is a reasonable assumption for the case study considered in this Section (see §5.1), where the assumed sea state population is representative of the North Atlantic Ocean.

Fig. 5 shows trajectories of cumulated damage as a function of the steepness of encountered sea states. Represented trajectories are restricted to long-term realizations which have led to failure (recall that  $P_{\text{fail}} = 2.3\%$  in the present case study); in total 20 realizations leading to failure are represented. To build each trajectory shown Fig. 5, encountered sea states – until failure occurrence – have been first collected and sorted in terms of sea state steepness (in descending order). Therefore, Fig. 5 is suitable for identifying predominant classes of damaging sea states, in terms of wave steepness. In the quadratic stress-response regime, some failure occurrences are due to the ultimate strength exceedance, rather than accumulated fatigue reaching unity; these cases are shown as empty circles in Fig. 5, right panel.

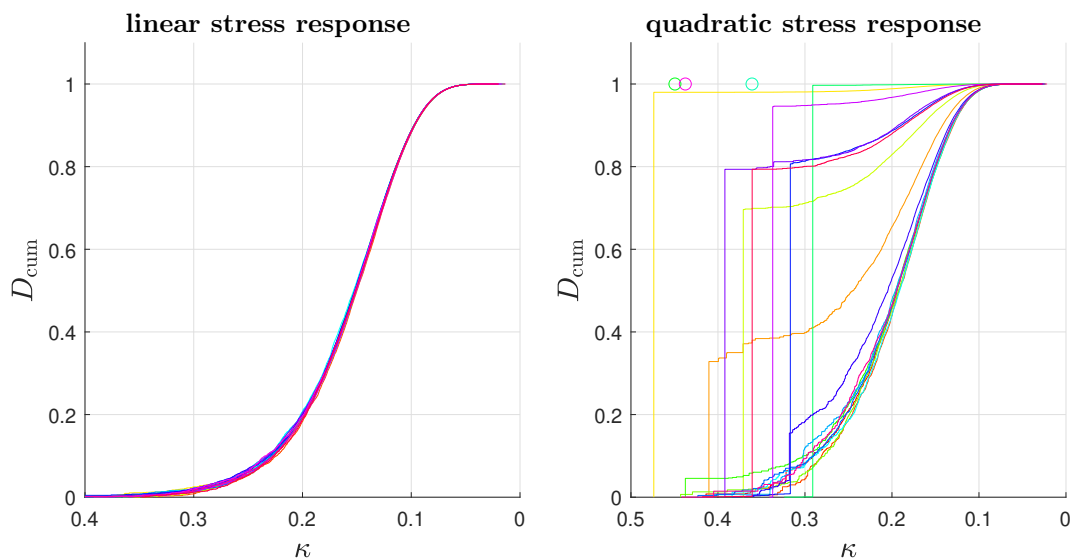


Figure 5: Cumulative damage to failure,  $D_{\text{cum}}$ , as a function of sea state wave steepness,  $\kappa$ . The number of represented failure realizations is  $N_{\text{rea}} = 20$ . Results are shown for the linear (left) and quadratic (right) stress-response regimes. On the right panel, empty circles are used to represent realizations where failure is due to ultimate strength exceedance; the position of the circle shows the wave steepness of the sea state responsible for the ultimate strength exceedance event. In the colour version, each failure realization is given a different colour.

In the linear stress-response regime, the curves  $D_{\text{cum}}(\kappa)$  show little dispersion. About 80% of the cumulated damage is generated by sea states which present wave steepness values within the range  $\simeq 0.098 - 0.23$ , i.e., relatively “common” steepness values. In the quadratic stress-response regime, the curves  $D_{\text{cum}}(\kappa)$  are much more dispersed. In this regime, realizations leading to failure can be divided into two classes:

1. A first class, in which the cumulated damage is built up over a large number of sea states, which individually contribute to a small fraction of the cumulated damage;
2. A second class where a single sea state contributes to a very large proportion of the cumulated

damage.

In Fig. 5, the realizations belonging to the latter class take two different forms: (i) curves showing large vertical jumps; (ii) curves reduced to a single point (represented as empty circles). The latter form corresponds to realizations where failure is due to ultimate strength exceedance.

### 5.3. Dominant class of damaging impacts

In continuity with the previous subsection, this one investigates which populations of water waves are predominant in terms of damage. The focus is on the nonlinearity degree of water waves. To characterize the nonlinearity level of impacting waves, the slope of the free surface, at impact, is one quantity of particular interest. Indeed, this quantity can be used as a proxy for the steepness of the impacting wave. Appendix C shows that the conditional mean of the free-surface slope – given the impact velocity,  $w$ , and the sea state properties – can be used as a reasonable proxy for the realized value of the free-surface slope. Hereinafter this conditional mean of the free-surface slope is denoted by  $E[\eta_{,x}|w]$ ; its expression is given in Appendix C, Eq. (C.3). Following Eq. (C.3),  $E[\eta_{,x}|w]$  is negative for  $w > 0$ , the latter being always satisfied for a free-surface upcrossing event (within the linear wave model).  $E[\eta_{,x}|w] < 0$  indicates that the conditional mean slope is downward in the direction of wave propagation.

Fig. 6 shows, for a sample of realizations leading to failure, the cumulative damage,  $D_{\text{cum}}$ , as a function of the mean conditional slope,  $E[\eta_{,x}|w]$ . To produce the plots in Fig. 6, for each realization leading to failure, the encountered impacts – until failure – have been collected and sorted in terms of conditional slope, in descending order (in absolute value).

In the linear stress-response regime, there is little scatter in the curves  $D_{\text{cum}}$  vs  $E[\eta_{,x}|w]$ . Approximately 80% of the cumulated damage leading to failure is due to waves with  $E[\eta_{,x}|w]$  lying within the range  $\simeq -16^\circ \rightarrow -6^\circ$ . These slopes can be converted into steepness values of “equivalent” regular waves through

$$k_{\text{reg}} A_{\text{reg}} \equiv |E[\eta_{,x}|w]|, \quad (21)$$

where  $k_{\text{reg}}$  and  $A_{\text{reg}}$  are the wave number and amplitude of the equivalent regular wave. The range of slopes  $\simeq -16^\circ \rightarrow -6^\circ$  correspond to a range of equivalent-wave steepness  $k_{\text{reg}} A_{\text{reg}} \simeq (0.089 \rightarrow 0.033) \times \pi$ . This range of steepness values corresponds to waves which are moderately nonlinear, and for which the linear wave model may represent a reasonable approximation. Conversely, in the quadratic stress-response regime, there is significant dispersion in the curves  $D_{\text{cum}}$  vs  $E[\eta_{,x}|w]$ . As in Subsection 5.2, realizations leading to failure can be categorized into two classes:

1. A first class, in which the cumulated damage is built up by a large number of impacts, which individually contribute to a small fraction of the cumulated damage.
2. A second class, in which a single impact contributes to a very large fraction of the cumulated damage. This is due to the fact that this single impact induces a first-cycle response which either exceeds the ultimate strength of the material (cases shown as empty circles in Fig. 6), or is not far below the ultimate strength ( $s^{(1)}/S_u \gtrsim 0.9$ ), leading to significant low cycle damage (curves with large vertical jumps in Fig. 6).

In the first class, most of the cumulated damage is built up by a large number of impacts with slopes (in absolute values) below  $20^\circ$ , which corresponds to equivalent regular waves with steepness values  $k_{\text{reg}} A_{\text{reg}} \lesssim 0.11\pi$ . In the second class, most impacts responsible for a large proportion of the cumulated damage have conditional mean slopes above  $30^\circ$ . Such large values mean that the linear wave framework is inappropriate to model this class of wave impacts (this point is further discussed in Section 6).

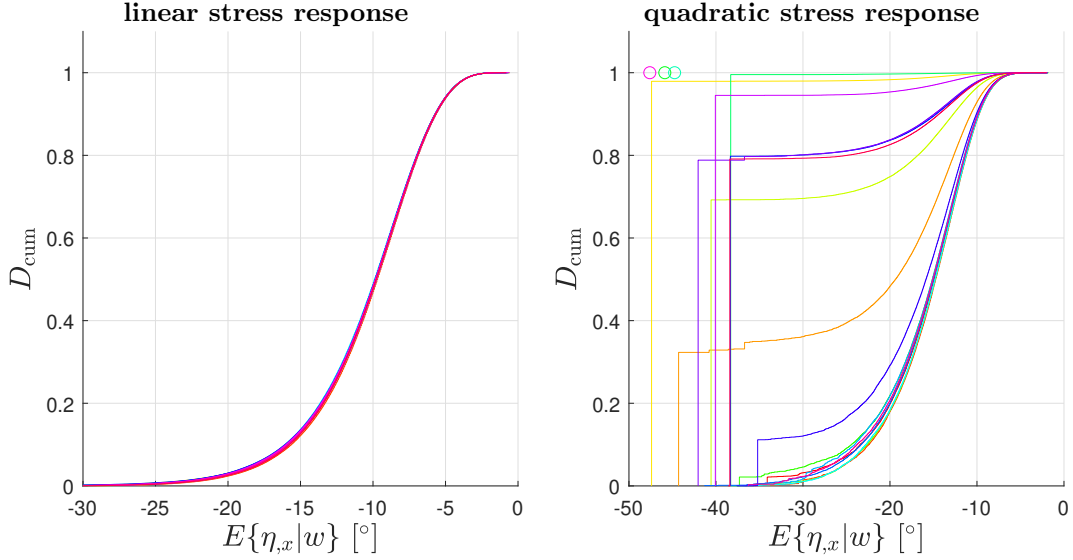


Figure 6: Cumulative damage as a function of the conditional mean of the free-surface slope,  $\eta_x$ , given the impact vertical velocity,  $w$ , and the sea state properties (see Eq. C.3). The number of represented realizations is  $N_{\text{rea}} = 20$ . Results are shown for the linear (left) and quadratic (right) vibratory stress-response regimes. On the right panel, empty circles are used to represent realizations where failure is due to ultimate strength exceedance; the position of the circle shows the conditional mean free-surface slope for the wave impact responsible for the ultimate strength exceedance event. In the colour version, each colour represents the same realization as in Fig. 5.

#### 5.4. Dominant damage channels

Fig. 7 shows how the damage leading to failure is distributed among the four different damage channels, which are the three fatigue regimes, plus the ultimate strength exceedance.

In the linear stress-response regime, no realized failure is due to the exceedance of the ultimate strength. The damage contribution from the low cycle regime is also effectively zero. Then, the cumulated fatigue damage is comparably distributed between the high cycle and very high cycle regimes.

In the quadratic dynamical regime, the two different classes of failure realizations identified in §5.2-5.3, are distinguishable again. In the first class (failure realizations where the bulk of damage is due to a large number of encountered sea states and resulting wave impacts) the fatigue damage is mostly built up in the high cycle regime, with secondary contributions from the very high cycle and low cycle regimes. In the second class (failure realizations where the damage is dominated by a single extreme wave impact) the damage leading to failure is either due to the exceedance of the ultimate strength, or fatigue mostly built up in the low cycle regime.

## 6. Discussion

The present section discusses the results presented above, in §6.1 for the linear vibratory stress-response regime, and in §6.2 for the quadratic vibratory stress-response regime. Then, the case of the quasistatic stress-response regime is specifically addressed in §6.3. Section 6.4 discusses the

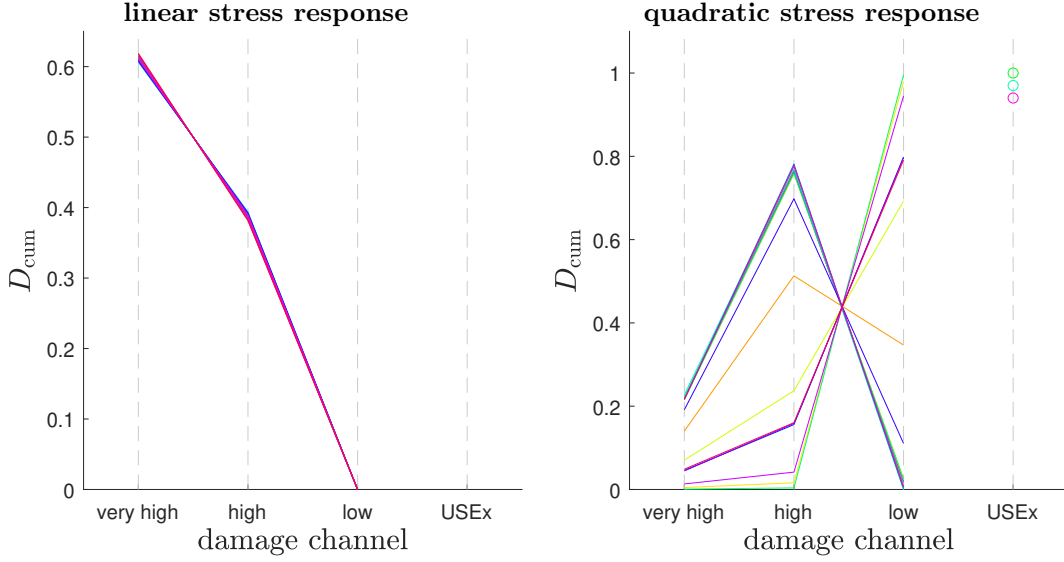


Figure 7: Contribution of the different damage channels leading to failure. The number of represented realizations is  $N_{\text{rea}} = 20$ . The labels “very high”, “high”, and “low” are used for the very high cycle, high cycle, and low cycle fatigue regimes, respectively. The fatigue damage contributions add up to unity. On the right panel, cases where failure is due to ultimate strength exceedance are shown as empty circles, on the vertical line labelled by “UEx”; for these cases, the fatigue damage, cumulated before the occurrence of the ultimate strength exceedance event, is not shown. Empty circles are slightly offset from each other, such that all failure realizations due to ultimate strength exceedance are made visible on the plot. In the colour version, each colour represents the same realization as in Figs. 5-6.

effects of a change in the elevation of the impacted body. Finally, §6.5 briefly explains how the main parameters of the model may be inferred for a specific structural element.

### 6.1. Linear vibratory stress-response regime

In the linear stress-response regime, the risk of failure due to fatigue yields structural-sizing constraints which are noticeably more conservative than the constraints derived from the risk of ultimate strength exceedance, alone. In the examples considered in Section 4, for a given (small) failure probability,  $P_{\text{fail}}$ , the structural sizing factor  $S_*$  is 2 to 5 times smaller (depending on the considered sea state configuration, exposure time, and modeling approach used for the  $SN$  curve randomness) when fatigue is included in the risk analysis. Effectively, in the linear stress-response regime, fatigue accumulation is the dominant failure mode to be considered when designing a marine structure against bottom wave slamming. The cumulated fatigue damage leading to failure is mostly built up in the high cycle and very high cycle regimes. The probability of a stress cycle reaching the low cycle branch is very small and may be considered to be null for practical purposes. The cumulated fatigue damage is built up by a large number of encountered sea states and wave impacts, which are rather “common”. As a result, the randomness of the realized long-term stress-cycle distribution is unimportant when modeling the risk of failure; the mean stress-cycle distribution is a proxy of sufficient accuracy to model the damage cumulated on the long-term

exposure. As a corollary, modeling the short-term serial dependence in encountered sea states is also of no importance, in the linear stress-response regime.

The cumulated damage is mostly due to sea states which have characteristic wave steepness values in the range  $\kappa \simeq 0.1 - 0.2$  (see Eq. 20 for the definition of  $\kappa$ ). Although these sea states are not particularly extreme, the effect of wave nonlinearities on level-crossing statistics is expected to be already substantial, for this range of wave cambers (see [51]). Nonlinearities will affect the predicted damage in two ways: (i) the frequency of wave impacts will be changed; and (ii) the conditional distribution of wave kinematics, given wave impact, will be also modified.

Different approaches could account for wave non-linearities in the risk analysis. To the second-order, the effect of wave nonlinearities, both on the impact frequency and on the conditional distribution of wave kinematics, may be semi-analytically approached by using Edgeworth series [51]. Edgeworth series are appropriate for modeling the bulk of level-crossing distributions, which is the relevant portion of distributions for fatigue analysis. Beyond the second order, another approach could be to build a library of upcrossing frequencies and conditional distributions, estimated for different sea state conditions. This library may be populated through experiments (in a lab or in the field), through simulations, or through a combination of both (with a multifidelity method). It should be noted that, for each sea state condition, the experiments (whether physical or numerical) would not need to be conducted over particularly long time frames, as the wave impacts responsible for fatigue damage are not excessively rare events. Then, a response model may be fitted to the library, and used as a replacement of the first-order wave model, in the long-term analysis. For instance, the recent database produced within the DeRisk project [52] may be particularly suitable to produce such a library.

## 6.2. Quadratic vibratory stress-response regime

In the quadratic stress-response regime, accounting for fatigue damage in the risk assessment is less critical than in the linear stress-response regime. Indeed, for the configurations considered in this study, the structural sizing factor,  $S_*$ , including the risk due to fatigue accumulation, is only 5-45% smaller (depending on the considered configuration) than the value obtained when only the risk of ultimate strength exceedance is accounted for. The scenario realizations leading to failure can be roughly divided into two classes. A first class where the cumulated fatigue damage is mostly built up by a very large number of encountered sea states, similarly to the situation observed in the linear stress-response regime. A second class where the damage leading to failure is dominated by a few extreme events. Due to the important weight of extreme sea states in the risk of failure, the serial dependence in the sequences of encountered sea states is found to have an effect on the predicted probability of failure,  $P_{\text{fail}}$ . However, the effect is found to be modest in the range of small  $P_{\text{fail}}$  values. The quadratic stress-response regime poses modeling challenges regarding at least two aspects:

1. The low cycle fatigue regime is found to play an important role in the risk of failure. In this study, the low cycle fatigue is modeled in a simplified manner. A more advanced approach (possibly considering time-history effects) would be necessary in order to accurately estimate the fatigue damage in the low cycle regime. Indeed, the use of Miner's rule may become particularly questionable for scenarios where loading amplitudes work intermittently in the low cycle and high cycle regimes.
2. Two different classes of wave impacts are “competing” in the risk of failure. The cumulated damage leading to failure, may be due to: a single, extreme impact (ultimate strength ex-

ceedance); a small number of extreme impacts combined with a large number of “milder” impacts; or a large number of wave impacts, with no single impact contributing to a very large proportion of the cumulated damage.

The proper modeling of extreme wave impacts (probability of occurrence and wave kinematics) would require a specific approach able to render the nonlinearity of the most extreme waves (possibly breaking; see, e.g., [53] for a recent probabilistic wave breaking model) generated by the most extreme sea states. This likely constitutes the most challenging aspect to accurately assess the risk of failure, in the quadratic stress-response regime.

### 6.3. Quasistatic regime

The case of the quasistatic regime has been mentioned in §2.1, but it has not been investigated in Sections 3-4-5; it is specifically discussed in this section. In the quasistatic regime, the magnitude of the stress response is expected to be proportional to the slamming load, but no significant vibratory excitation is expected. Each wave impact would induce a single loading cycle (the picture may be more complicated for bodies prone to secondary impact episodes; see footnote 1), whose amplitude is proportional to the impact velocity squared. This situation is similar to the one encountered in the quadratic vibratory regime, except for the sequence of decaying cycles, which is absent in the quasistatic case. Other things equal, this difference means that the weight of fatigue damage in the risk of failure will be diminished, with respect to the weight of ultimate stress exceedance. As shown in Appendix D, in the case of a power-law  $SN$  curve, the damage “amplification” due to the sequence of decaying cycles, is rendered by a factor  $(1 - \exp\{-2\pi\zeta q\})^{-1}$  (see Eq. D.4), where  $q$  is the  $SN$  curve power-law index, and  $\zeta$  the vibration damping ratio. To give an order of magnitude, for  $\zeta = 10^{-2}$  and  $q = m = 3$  (index assumed for the high cycle branch), this factor equals  $(1 - \exp\{-2\pi\zeta q\})^{-1} \simeq 5.8$ . The absence of this amplification factor in the quasistatic regime, has the effect of suppressing the class of long-term realizations, where the damage leading to failure is mostly built up by a large number of cumulated impacts (see §5.3, where this class was denoted as the “first” class). Hence, fatigue damage becomes barely relevant in the risk of failure, within the range  $P_{\text{fail}} \lesssim 5\%$  (this has been verified numerically).

### 6.4. Effect of the elevation of the exposed body

A final point that needs to be discussed is the effect of the elevation of the exposed body on the weight of fatigue damage relative to the ultimate strength limit, in the risk of failure. For purposes of simplicity, in the examples considered in Sections 4-5, the control material point – representing the exposed body – has been assumed to lie at the mean water level; consequently, all waves trigger slamming events.

When the control material point is moved away from the mean water level (either above or below), only the waves sufficiently large to induce free-surface crossing events will lead to slamming events. Hence, as the absolute value of the material point elevation,  $|a|$ , increases, slamming events become less frequent and tend to increasingly select high waves and large- $H_s$  sea states (see Eq. 16, which gives the mean number of slamming events for a given sea state). Then, as  $|a|$  increases, the ultimate strength limit is expected to gain in importance relative to fatigue damage in the risk of failure. For the quadratic vibratory response regime (see §6.2) and the quasistatic regime (see §6.3), this means that an increase in  $|a|$  will further enhance the conclusion that fatigue damage is moderately to marginally relevant in the risk analysis.

In the linear vibratory stress-response regime (see §6.1), it has been found that the risk related to fatigue damage can lead to sizing constraints that are significantly more conservative than the

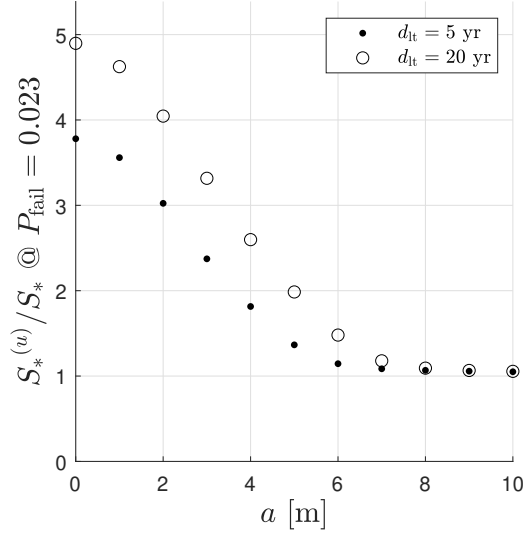


Figure 8: Effect of the elevation of the body. This figure shows the ratio  $S_*^{(u)}/S_*$  as a function of the elevation of the body, for a failure probability fixed to  $P_{fail} = 0.023$ . Results are shown for two exposure durations:  $d_{lt} = 5$  yr (dots);  $d_{lt} = 20$  yr (empty circles). Further details can be found in the main body of the text.

ones obtained from the risk of ultimate strength exceedance. As the control point is moved away from the mean water level, this conclusion will not hold anymore, at some point. Indeed, in the most extreme case where  $|a|$  is increased to the point that the mean number of wave impacts become small over the exposure duration, fatigue is not relevant in the risk of failure, since the number of cumulated stress cycles is necessarily limited. To apprehend the order of magnitude of  $a$ , for which there is a change in the nature of the risk, numerical simulations have been carried out for different values of  $a$ . For this specific investigation, sea states are sampled from the North Atlantic population with a stationarity duration  $d_{st} = 1$  hr (population labelled as **sse-4** in Tab. 1). For this configuration, Fig. 8 shows the ratio  $S_*^{(u)}(P_{fail})/S_*(P_{fail})$ , for a failure probability fixed to  $P_{fail} = 0.023$ . As a reminder,  $S_*(P_{fail})$  is the structural sizing factor which includes the risk related to fatigue damage, and  $S_*^{(u)}(P_{fail})$  is the structural sizing factor obtained when only the risk of ultimate strength exceedance is accounted for. Fig. 8 shows a gradual decrease in  $S_*^{(u)}/S_*$ , as the elevation of the body is increased. For an exposure duration  $d_{lt} = 20$  yr (resp.  $d_{lt} = 5$  yr), Fig. 8 shows that  $S_*^{(u)}(P_{fail})/S_*(P_{fail})$  falls below 1.2 for  $a \simeq 6.9$  m (resp.  $a \simeq 5.8$  m).

#### 6.5. On the inference of the main model parameters for a specific structural element

The intent of this study has been to investigate whether it is necessary to consider fatigue damage as a relevant failure mode, when sizing a structural element exposed to bottom wave slamming. For this purpose, a simplified formulation has been introduced in Section 2.1, where the body structure is characterized by its vibratory response time (period of the first natural mode),  $t_{vib}$ , and the scale of the stress response to a wave impact,  $S_*$  (introduced in Eq. 3). The curves showing  $P_{fail}$  as a function of  $S_*$ , as exemplified in Fig. 3, may be used to estimate the probability of failure for a given structural element. For this purpose, as a first step, the characteristic timescales  $t_{on}$ ,  $t_{imp}$  and  $t_{vib}$



need to be estimated, for the structural element under study. The timescales  $t_{\text{on}}$ ,  $t_{\text{imp}}$  are related to the time evolution of the slamming loads during a wave impact. These timescales should be evaluated for a range of impact velocities representative of the vertical fluid velocities encountered in water waves (i.e. a few  $\text{m} \cdot \text{s}^{-1}$ ), from water-entry experiments or numerical simulations. The vibratory response timescale (i.e. the eigen frequency of the dominant structural mode),  $t_{\text{vib}}$ , may be obtained from a modal analysis, including the added-mass effect. Then, the stress response regime relevant to the structural element can be identified from the characteristic times  $t_{\text{on}}$ ,  $t_{\text{imp}}$ ,  $t_{\text{vib}}$ . If the stress-response is quasistatic ( $t_{\text{vib}} \ll t_{\text{on}}$ ), the risk of failure due to fatigue damage is not expected to be more restrictive – in terms of structural sizing – than the risk of ultimate strength exceedance (see §6.3). If  $t_{\text{vib}} \simeq t_{\text{on}}$  or  $t_{\text{vib}} \simeq t_{\text{imp}}$ , no single asymptotic stress-response regime can be clearly identified, and the present simplified approach is not applicable (as discussed in §2.1). In the other cases (i.e.  $t_{\text{on}} \ll t_{\text{vib}} \ll t_{\text{imp}}$  or  $t_{\text{vib}} \gg t_{\text{imp}}$ ), the stress-response factor  $S_*$  – for a particular detail of the structural element – may be estimated by performing numerical simulations or lab experiments of the water entry of the structural element. Then, the probability of failure may be estimated from curves such as those shown in Fig. 3.

## 7. Summary and conclusions

Within the context of the risk of failure induced by bottom wave slamming on marine structures, the main purpose of this study has been to investigate whether fatigue damage can be a relevant failure mode (i.e., can lead to structural sizings being significantly more conservative) with respect to the risk of ultimate strength exceedance. Without further specifications, the impacted body has been assumed to have a shape prone to a rapid rise of the hydrodynamic load at the beginning of the impact, ensuring a vibratory excitation of the structure (this is typically the case for blunt bodies). Two asymptotic stress-response regimes have been investigated:

- A first regime, in which the vibratory-response timescale of the structure is much shorter than the impact-load timescale,  $t_{\text{vib}} \ll t_{\text{imp}}$ . In this first regime, the structural stress is expected to quadratically respond to the impact velocity;
- A second opposite regime,  $t_{\text{vib}} \gg t_{\text{imp}}$ , in which the structural stress is expected to linearly respond to the impact velocity.

The sizing of the structure is modeled through a sizing factor,  $S_*$ , which sets the magnitude of the stress response, assuming that it is dominated by a single vibratory mode. The  $SN$  curve pattern used in this study is an extended version of the fatigue curves recommended by classification societies for the high cycle and very high cycle regimes. To combine the risks due to fatigue and due to the ultimate strength exceedance, the  $SN$  curve pattern is extended to the low cycle regime, up to the ultimate strength of the material.

In the linear vibratory stress-response regime, fatigue damage is found to be a failure mode important to consider when designing a marine structure. For a given failure probability, it yields constraints on the sizing factor,  $S_*$ , which are significantly more conservative (by a factor 2 to 5, in the examples considered in this study) than the constraints obtained from the risk of ultimate strength exceedance only. Conversely, in the quadratic vibratory stress-response regime, the additional degree of conservativeness brought by the consideration of fatigue damage (with respect to the risk of ultimate strength exceedance alone) is found to be more modest. However, this result comes with the caveat that low-cycle fatigue damage is found to play an important role, which

makes the use of Miner’s rule subject to caution. Besides, extreme sea states and extreme waves play an important role in the risk of failure, which questions the use of the linear wave model.

A more advanced analysis, taking into account wave nonlinearities, together with a more advanced model of fatigue damage, may be the subject of a future study. Also, it would be interesting to investigate how the use of a more advanced and more specific hydroelasticity model may confirm or change the conclusions of the present study. A more advanced hydroelasticity model would enable the consideration of multiple vibratory modes in the fatigue analysis, and it would enable the exploration of the transitional stress-response regimes where  $t_{\text{vib}} \simeq t_{\text{on}}$  or  $t_{\text{vib}} \simeq t_{\text{imp}}$ .

## Appendix A. Effect of cycle mean stresses

This appendix discusses the potential effect of cycle mean stresses on fatigue damage estimates, and the related risk of failure. Cycle mean stresses are expected to be small in the impulsive regime (see right panel in Fig. 1); therefore, in this regime, a significant effect of cycle mean stresses is not expected. Conversely, the magnitude of cycle mean stresses is expected to be comparable with the magnitude of cycle stress amplitudes, both in the quasistatic regime (left panel in Fig. 1), and the quadratic vibratory stress-response regime (middle panel in Fig. 1). For discussion purposes, let us consider the Goodman relation (see, e.g., [31]), which proposes to take into account the cycle mean stresses as follows:

$$\tilde{S}(N) = S(N) [1 - S_{\text{m}}/S_{\text{u}}] , \quad (\text{A.1})$$

where  $S(N)$  is the zero-mean-stress  $SN$  curve, and  $\tilde{S}(N)$  is the modified  $SN$  curve for a mean stress equal to  $S_{\text{m}}$ . Both in the quasistatic and in the quadratic vibratory stress-response regimes, as a first approximation, it can be assumed that the mean stress is comparable to the amplitude of the first cycle following impact,  $S_{\text{m}} \simeq s^{(1)}$ . It should be noted that there is only one cycle per impact in the quasistatic regime, if the hydrodynamic load monotonically decreases after the onset. Then, by setting  $s^{(1)} = \tilde{S} = S_{\text{m}}$  into Eq. (A.1), and differentiating, the following relation is obtained:

$$\frac{d\tilde{S}}{dS} \simeq \frac{1}{(1 + S/S_{\text{u}})^2} . \quad (\text{A.2})$$

In essence, Eq. (A.2) shows that the effect of the mean stress is to “compress” (i.e.  $d\tilde{S}/dS < 1$ ) the range of stress amplitudes where fatigue damage works. From a risk-of-failure perspective, this means that the weight of fatigue-related risk will be reduced, relatively to the risk of ultimate strength exceedance. This point has been numerically verified for the quadratic vibratory stress-response regime, assuming that for each impact the mean stress is equal to  $S_{\text{m}} = s^{(1)}$ , and that it does not evolve during the vibratory response. A Gerber-type model [31] – where  $[1 - S_{\text{m}}/S_{\text{u}}]$  would be replaced by  $[1 - (S_{\text{m}}/S_{\text{u}})^2]$  in Eq. (A.1) – would produce a similar effect, although it would be less pronounced.

## Appendix B. Storm resampling method

The storm resampling method, used in the present study, has been proposed and detailed by Mackay and Jonathan (2020) [46]. This appendix sketches the principle of the method, and provides some elements of validation for the version implemented in the present study.

### Appendix B.1. Principle of the method

The bottom line of the storm resampling method is that it divides the historical time series into storm blocks. Here, a “storm” is defined by a time interval, within which a local maximum significant steepness can be identified, where the sea state steepness is defined by Eq. (20), which differs from the steepness definition used in [46] (but only by a proportionality factor). A “storm” does not need to contain severe sea state conditions and may actually cover a period of calm. Blocks are adjoining (no data in the time series is ignored), and the steepness maxima of two successive storms are required to be separated by a minimum time interval of 5 days. The minimum separation of 5 days ensures that the resulting population of storms can be reasonably considered as serially independent.<sup>6</sup> Following this latter constraint, a storm block may actually contain several local maxima of wave steepness. Then, the population of storms is modeled by a two-dimensional probability distribution, in terms of two storm particulars,  $\kappa_p$  and  $d_p$ . The storm particular  $\kappa_p$  is the peak wave steepness of the storm. The second storm particular,  $d_p$ , is the peak value of the auxiliary variable

$$d = \sqrt{\left(\frac{H_s}{1\text{ m}}\right)^2 + \frac{1}{2} \left(\frac{T_z}{1\text{ s}}\right)^2}. \quad (\text{B.1})$$

The sample of empirical particular couples,  $(\kappa_p, d_p)^{(e)}$ , is fitted by using a composite approach: a kernel density approach for the body of the distribution; the conditional extremes model of Heffernan & Tawn (2004) [54] for the high-value tails.

Then, a realized synthetic sequence of sea states is obtained by drawing a sequence of independent synthetic storms, where each storm is simulated as follows:

1. A synthetic couple of particulars,  $(\kappa_p, d_p)^{(s)}$ , is drawn from the fitted distribution.
2. From a subset of observed storms – whose particulars,  $(\kappa_p, d_p)^{(e)}$ , are sufficiently close to the synthetic particulars,  $(\kappa_p, d_p)^{(s)}$  – a storm candidate is selected at random.
3. The hourly  $\kappa$ –series and  $d$ –series of the selected storm candidate are rescaled, respectively by the factors  $\kappa_p^{(s)}/\kappa_p^{(e)}$  and  $d_p^{(s)}/d_p^{(e)}$ , to produce the synthetic storm.

The reader is referred to Mackay and Jonathan (2020) [46] for further details about the procedure.

### Appendix B.2. Validation of the implemented version

Based on the original proposal put forward by Mackay and Jonathan (2020) [46], the storm resampling method has been implemented for the purpose of the present study. The dataset, used in the present work, consists of 10 years of buoy measurements acquired in the Gulf of Maine (labelled as “dataset A” in [44]). This dataset is the same as the one used in [46], which eased comparisons and validation. Below, some elements of validation of this implemented version are provided.

Fig. B.1, left panel, compares – in the  $(T_z, H_s)$  plane – the 10 years of observed sea states with 50 years of synthetic sea states. The right panel of Fig. B.1 compares the observed scatter plot of storm particulars,  $(s_p, d_p)$ , with its synthetic counterpart. As an additional piece of information,

---

<sup>6</sup>Except for the seasonal modulation, which makes severe conditions more probable in winter than in summer for the considered US coast site. However, the seasonal modulation does not need to be explicitly modeled, as long as the exposure duration is supposed to be continuous and to span several years.

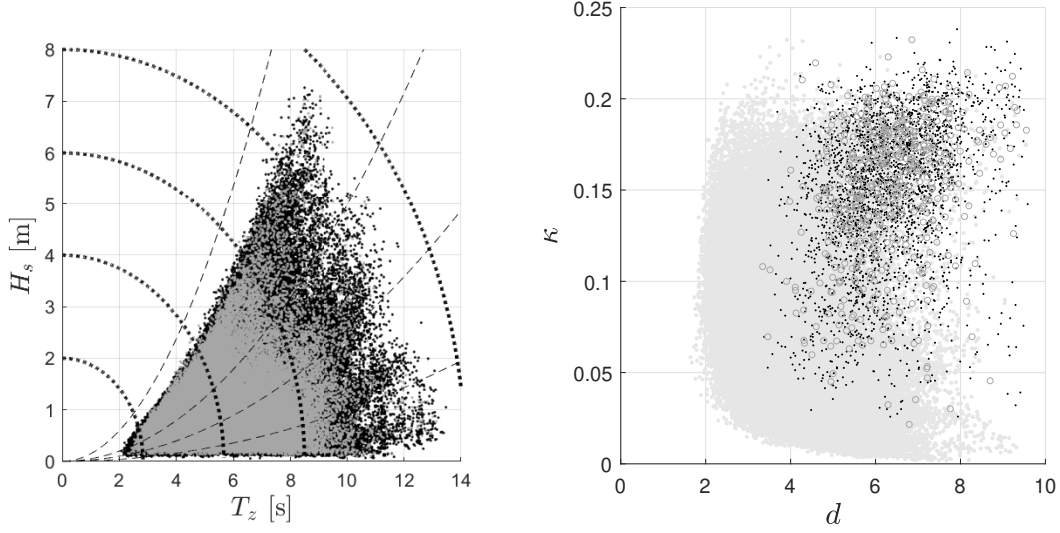


Figure B.1: Storm resampling method – scatter plots. Left: scatter plot of sea states in the plane  $(T_z, H_s)$ . Observed (resp. simulated) sea states are shown as grey (resp. black) dots. Grey dots overlay black dots. Isovalue lines for the auxiliary variables  $d$  and  $\kappa$  are shown as dotted lines and dashed lines, respectively. The values along the iso- $d$  (resp. iso- $\kappa$ ) lines are 2; 4; 6; 8; 10 (resp. 0.02; 0.05; 0.1; 0.3). Right: scatter plot of the storm particulars,  $d_p$  and  $\kappa_p$ . Simulated storms are shown as black dots. Observed storms are shown as dark-grey empty circles. The whole population of observed sea states is also shown as light-grey dots. The realized synthetic storm sample is the same on both panels. The total duration of simulated sea states is 5 times larger than the duration of observed sea states; i.e. the simulated data span 50 yr.

the whole population of observed sea states, in the plane  $(d, s)$ , is also shown in the right panel of Fig. B.1.

Fig. B.2 offers a different impression of the model performance (especially for extreme events) by comparing the observed and synthetic marginal distributions obtained for the sea state particulars  $H_s$  and  $T_z$ . In Fig. B.2, the amount of simulated data (1000 years) has been taken sufficiently large to ensure that the statistical fluctuations are very small in the synthetic distributions. It has been checked that the differences between the observed and synthetic distributions are compatible with the magnitude of sampling uncertainties due to the limited duration of observed sea states.

### Appendix C. Proxy for impacting-wave slopes

This appendix shows that the conditional mean of the local free-surface slope – given the impact velocity,  $w$ , and the sea state characteristics,  $H_s$  and  $T_z$  – can be used as a relevant proxy for the slopes of impacting waves. For this purpose, a two-dimensional frequency-direction wave spectrum is assumed:

$$G(\omega, \theta) = \mathcal{A}(\theta)\mathcal{S}(\omega), \quad (\text{C.1})$$

where  $G$  denotes the two-dimensional wave spectrum,  $\omega$  the wave angular frequency, and  $\theta$  the wave direction of propagation. In Eq. (C.1), the frequency and direction dependencies have been

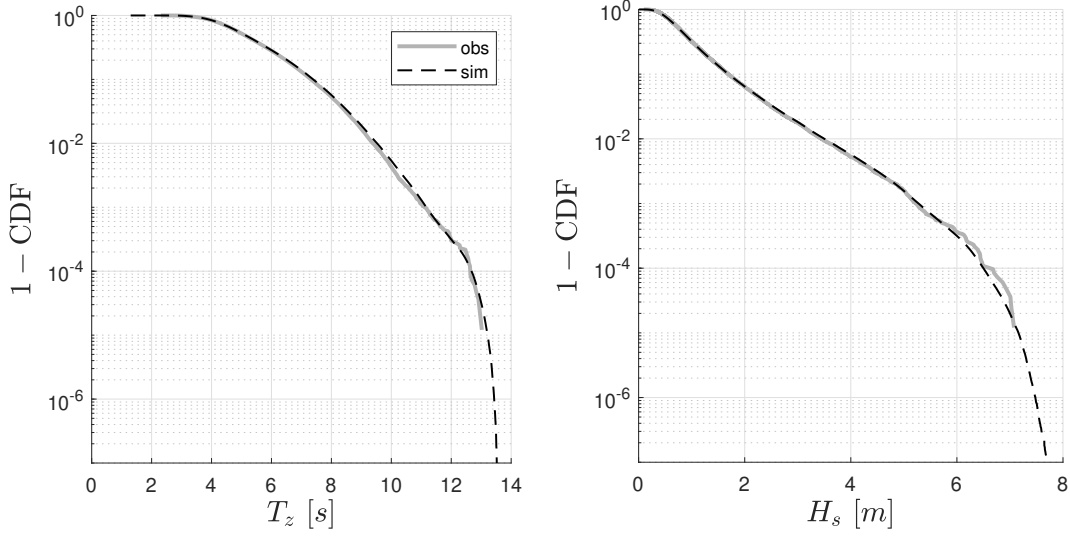


Figure B.2: Storm resampling method – Marginal distributions (exceedance probability) of  $T_z$  and  $H_s$ . The empirical distributions derived from buoy measurements are shown as solid grey lines. The distributions obtained from the storm resampling method are shown as dashed black lines. Left: distributions of  $T_z$ . Right: distributions of  $H_s$ .

assumed to be separable, with  $\mathcal{S}$  being the one-sided wave frequency spectrum, and  $\mathcal{A}$  the wave direction distribution; the function  $\mathcal{A}$  satisfies

$$\int_{-\pi}^{\pi} d\theta \mathcal{A}(\theta) = 1. \quad (\text{C.2})$$

The slope along the average wave direction,  $\theta = \theta_0$ , will be noted  $\eta_{,x}$  and it will be used as a proxy for the steepness of the impacting waves. Thus far, a wave impact has been specified solely through the vertical velocity of the fluid,  $w$ , at impact; the wave slope is not used as an input of the simplified structural response model adopted in this study. Within the linear wave model,  $\eta_{,x}$  and  $w$ , non-conditioned to level-crossing, are jointly Gaussian, and are both independent of the free-surface elevation  $\eta$  (see for instance Section 3.1 in [29]). Then it follows that the conditional distribution of  $\eta_{,x}$ , given  $w$ , is also Gaussian. The conditional mean and conditional variance are given by

$$E[\eta_{,x}|w] = \rho \sigma_{\eta_{,x}} \frac{w}{\sigma_w}, \quad (\text{C.3})$$

and

$$\text{Var}[\eta_{,x}|w] = \sigma_{\eta_{,x}}^2 (1 - \rho^2), \quad (\text{C.4})$$

where  $\rho$  is the nonconditional correlation coefficient between  $\eta_{,x}$  and  $w$ . The nonconditional standard deviation of the vertical fluid velocity,  $\sigma_w$ , is given by Eq. (14). Assuming infinite water depth, the nonconditional standard deviation of  $\eta_{,x}$  is given by (see Section 3.1 in [29])

$$\sigma_{\eta_{,x}}^2 = \alpha_2 \frac{m_4}{g^2}, \quad (\text{C.5})$$

and the correlation coefficient is given by

$$\rho\sigma_{\eta,x}\sigma_w = E[\eta_{,x}w] = -\alpha_1 \frac{m_3}{g}. \quad (\text{C.6})$$

In Eqs. (C.5-C.6),  $g$  is the acceleration due to gravity, the third- and fourth-order wave moments,  $m_3$  and  $m_4$ , are defined by

$$m_p = \int_0^{+\infty} \omega^p S(\omega) d\omega, \quad (\text{C.7})$$

and the coefficients  $\alpha_1$  and  $\alpha_2$  depend on the wave direction distribution as follows:

$$\alpha_p = \int_{-\pi}^{\pi} d\theta \mathcal{A}(\theta) \cos^p \theta. \quad (\text{C.8})$$

Note that  $E[\eta_{,x}|w]$  and  $\text{Var}[\eta_{,x}|w]$  depend on the sea state spectrum through  $\sigma_{\eta,x}$  and  $\sigma_w$ ; this dependency is kept implicit in Eqs. (C.3-C.4). Here, for the sake of simplicity, all sea states are assumed to have the same shape of two-dimensional wave spectrum. The wave direction distribution is assumed to be of “cosine-squared” type:

$$\mathcal{A}(\theta) = \begin{cases} (2/\pi) \cos^2 \theta & , \text{ for } |\theta| < \pi/2 \\ 0 & , \text{ for } |\theta| > \pi/2, \end{cases} \quad (\text{C.9})$$

with an average propagation direction  $\theta_0 = 0$ . The wave frequency spectrum is assumed to have a JONSWAP shape [55], with a narrowness parameter  $\gamma = 3.3$ . Besides, 1% of the wave energy is truncated at low and high frequency (in total 2% of wave energy is discarded). The high-frequency truncation ensures that the variance of the free-surface slope is finite. The spectrum is normalized following Eq. (12), *after* the truncation operation. Eqs. (C.5-C.9) can be used to numerically compute the correlation coefficient:

$$\rho \simeq -0.922. \quad (\text{C.10})$$

The ratio of conditional mean and standard deviation is given by

$$\frac{E[\eta_{,x}|w]}{\sqrt{\text{Var}[\eta_{,x}|w]}} = \frac{\rho}{\sqrt{1-\rho^2}} \frac{w}{\sigma_w}. \quad (\text{C.11})$$

In the linear stress-response regime,  $\simeq 95\%$  (resp.  $\simeq 50\%$ ) of the cumulated damage is built up by impacts whose velocities are such that  $w/\sigma_w > 1.4$  (resp.  $w/\sigma_w > 2.4$ ). In the quadratic stress-response regime, damage-dominant impacts are biased to even larger values of  $w/\sigma_w$ . Using Eqs. (C.10-C.11),  $w/\sigma_w > 1.4$  translates into  $E[\eta_{,x}|w]/\sqrt{\text{Var}[\eta_{,x}|w]} < -3.3$ , which means that the relative dispersion around the mean of  $\eta_{,x}|w$  can be considered as moderate. Then, it follows that  $E[\eta_{,x}|w]$  can be used as a relevant proxy for the realized slope  $\eta_{,x}|w$ .

#### Appendix D. Damage induced by a single impact, assuming a power-law $SN$ curve

Following the assumptions introduced in Section 2, this appendix derives the fatigue damage induced by a wave impact, given its velocity  $w$ , in the case where the  $SN$  curve is modeled as a single power-law, as follows:

$$n(s) = n_0 \left( \frac{s}{S_0} \right)^{-q}, \quad (\text{D.1})$$

where  $q$  is a fixed power-law index, and  $n_0$  is the number of cycles to failure at the stress-cycle amplitude  $S_0$  (here the randomness of the  $SN$  curve is not considered). By combining Eqs. (2-6-D.1), the damage induced by a given impact can be expressed as:

$$D_{\text{imp}}(s^{(1)}) = \frac{1}{n_0} \left( \frac{s^{(1)}}{S_0} \right)^q \times \frac{1}{1 - \exp\{-2\pi\zeta q\}}. \quad (\text{D.2})$$

Then by using Eq. (3), the damage induced by a wave impact can be expressed as a function of the impact velocity,  $w$ , as follows:

$$D_{\text{imp}}(w) = D_* \left( \frac{w}{1 \text{ m/s}} \right)^{q \cdot r}, \quad (\text{D.3})$$

with

$$D_* = \frac{1}{n_0} \left( \frac{S_*}{S_0} \right)^q \frac{1}{1 - \exp\{-2\pi\zeta q\}}. \quad (\text{D.4})$$

## References

- [1] P. Temarel, W. Bai, A. Bruns, Q. Derbanne, D. Dessi, S. Dhavalikar, N. Fonseca, T. Fukasawa, X. Gu, A. Nestegård, A. Papanikolaou, J. Parunov, K. Song, S. Wang, Prediction of wave-induced loads on ships: Progress and challenges, *Ocean Engineering* 119 (2016) 274–308. doi:10.1016/j.oceaneng.2016.03.030.
- [2] Y. Dong, Y. Garbatov, C. Guedes Soares, Review on uncertainties in fatigue loads and fatigue life of ships and offshore structures, *Ocean Engineering* 264 (2022) 112514. doi:10.1016/j.oceaneng.2022.112514.
- [3] W. Mao, J. W. Ringsberg, I. Rychlik, G. Storhaug, Development of a fatigue model useful in ship routing design, *Journal of Ship Research* 54 (04) (2010) 281–293.
- [4] I. M. V. Andersen, J. J. Jensen, Hull girder fatigue damage estimations of a large container vessel by spectral analysis, *Proceedings of the PRADS2013* 20 (2013) 25.
- [5] B. Sweetman, S. R. Winterstein, Non-gaussian air gap response models for floating structures, *Journal of engineering mechanics* 129 (3) (2003) 302–309.
- [6] D.-H. Lim, Y. Kim, Probabilistic analysis of air gap of tension-leg platforms by a nonlinear stochastic approach, *Ocean Engineering* 177 (2019) 49–59. doi:10.1016/j.oceaneng.2019.02.054.
- [7] O. M. Faltinsen, *Hydrodynamics of High-Speed Marine Vehicles*, Cambridge University Press, 2006. doi:10.1017/CB09780511546068.
- [8] O. M. Faltinsen, Hydroelastic slamming, *Journal of Marine Science and Technology* 5 (2000) 49–65.
- [9] O. M. Faltinsen, Water entry of a wedge by hydroelastic orthotropic plate theory, *Journal of ship research* 43 (03) (1999) 180–193.

- [10] A. Tassin, M. Prevosto, R. Hascoët, N. Jacques, J.-C. Poirier, S. Seng, Y.-M. Scolan, J.-J. Maisonneuve, Essais d'impacts hydrodynamiques sur un aileron [in French], in: 18èmes Journées de l'Hydrodynamique, 2022, pp. 1–13.  
URL <https://jh2022.sciencesconf.org/419918/document>
- [11] A. Korobkin, T. Khabakhpasheva, Plane linear problem of the immersion of an elastic plate in an ideal incompressible fluid, *Journal of applied mechanics and technical physics* 40 (3) (1999) 491–500.
- [12] Y.-M. Scolan, Hydroelastic behaviour of a conical shell impacting on a quiescent-free surface of an incompressible liquid, *Journal of Sound and Vibration* 277 (1-2) (2004) 163–203.
- [13] H. Sun, O. M. Faltinsen, Water impact of horizontal circular cylinders and cylindrical shells, *Applied Ocean Research* 28 (5) (2006) 299–311.
- [14] K. J. Maki, D. Lee, A. W. Troesch, N. Vlahopoulos, Hydroelastic impact of a wedge-shaped body, *Ocean Engineering* 38 (4) (2011) 621–629.
- [15] D. J. Piro, K. J. Maki, Hydroelastic analysis of bodies that enter and exit water, *Journal of Fluids and Structures* 37 (2013) 134–150.
- [16] A. Iafrati, S. Grizzi, Cavitation and ventilation modalities during ditching, *Physics of Fluids* 31 (5).
- [17] S. Wang, C. Guedes Soares, Slam induced loads on bow-flared sections with various roll angles, *Ocean Engineering* 67 (2013) 45–57. doi:10.1016/j.oceaneng.2013.04.009.
- [18] C. Monroy, S. Seng, L. Diebold, A. Benhamou, Y. Jus, D. Le Touzé, G. Oger, et al., Comparative study of different methods for water impact computation, in: The 26th International Ocean and Polar Engineering Conference, 2016.
- [19] H. Xie, H. Ren, B. Deng, H. Tang, Experimental drop test investigation into slamming loads on a truncated 3D bow flare model, *Ocean Engineering* 169 (2018) 567–585. doi:10.1016/j.oceaneng.2018.10.003.
- [20] M. K. Ochi, L. E. Motter, Prediction of slamming characteristics and hull responses for ship design, *Trans. SNAME* 81 (1973) 144–176.
- [21] P. Rassinot, A. E. Mansour, Ship Hull Bottom Slamming, *Journal of Offshore Mechanics and Arctic Engineering* 117 (4) (1995) 252–259. doi:10.1115/1.2827231.
- [22] G. Wang, S. Tang, Y. Shin, A direct calculation approach for designing a ship-shaped FPSO's bow against wave slamming load, in: The Twelfth International Offshore and Polar Engineering Conference, International Society of Offshore and Polar Engineers, 2002, pp. 35–42.
- [23] O. Hermundstad, T. Moan, Efficient calculation of slamming pressures on ships in irregular seas, *Journal of Marine Science and Technology* 12 (2007) 160–182. doi:10.1007/s00773-006-0238-1.
- [24] S. Wang, C. Guedes Soares, Experimental and numerical study of the slamming load on the bow of a chemical tanker in irregular waves, *Ocean Engineering* 111 (2016) 369 – 383. doi:10.1016/j.oceaneng.2015.11.012.



- [25] Y.-M. Sclan, A. Korobkin, Water entry of a body which moves in more than six degrees of freedom, *Proceedings of the Royal Society A: Mathematical, Physical and Engineering Sciences* 471 (2015) 20150058.
- [26] J. B. Helmers, H. Sun, T. Landet, T. Driveklepp, Stochastic analysis of impact loads on marine structures, *International Conference on Offshore Mechanics and Arctic Engineering Volume 1: Offshore Technology* (2012) 659–670. doi:10.1115/OMAE2012-83849.
- [27] R. Hascoët, N. Jacques, Y.-M. Sclan, A. Tassin, A two-dimensional analytical model of vertical water entry for asymmetric bodies with flow separation, *Applied Ocean Research* 92 (2019) 101878. doi:10.1016/j.apor.2019.101878.
- [28] R. Hascoët, M. Prevosto, N. Raillard, N. Jacques, A. Tassin, Stochastic Prediction of Wave Impact Kinematics and Loads for Ship Appendages, in: *17èmes Journées de l’Hydrodynamique*, 2020, pp. 1–9.  
URL <http://website.ec-nantes.fr/actesjh/images/17JH/Articles/S02-2.pdf>
- [29] R. Hascoët, N. Raillard, N. Jacques, Effect of forward speed on the level-crossing distribution of kinematic variables in multidirectional ocean waves, *Ocean Engineering* 235 (2021) 109345. doi:10.1016/j.oceaneng.2021.109345.
- [30] J. Bannantine, J. Comer, J. Handrock, *Fundamentals of metal fatigue analysis*, Englewood Cliffs, NJ, Prentice Hall, 1990, 286.
- [31] R. I. Stephens, A. Fatemi, R. R. Stephens, H. O. Fuchs, *Metal fatigue in engineering*, John Wiley & Sons, 2000.
- [32] Bureau Veritas, NI-611-DT-R01-E, *Guidelines for fatigue assessment of ships and offshore units*, 2020.
- [33] Det Norske Veritas, DNV-CG-0129, *Fatigue assessment of ship structures*, 2021.
- [34] American Bureau of Shipping, *Guide for spectral-based fatigue analysis for vessels*, 2017.
- [35] Bureau Veritas, NR-216, *Rules on materials and welding for the classification of marine units*, 2021.
- [36] Det Norske Veritas, DNV-RU-SHIP-Pt2Ch2, *Materials and welding, Metallic materials*, 2021.
- [37] American Bureau of Shipping, *Rules for materials and welding*, 2022.
- [38] Y. Liu, S. Mahadevan, Stochastic fatigue damage modeling under variable amplitude loading, *International Journal of Fatigue* 29 (6) (2007) 1149–1161. doi:10.1016/j.ijfatigue.2006.09.009.
- [39] D. Paolino, M. Cavatorta, On the application of the stochastic approach in predicting fatigue reliability using miner’s damage rule, *Fatigue & Fracture of Engineering Materials & Structures* 37 (1) (2014) 107–117.
- [40] H. Shen, J. Lin, E. Mu, Probabilistic model on stochastic fatigue damage, *International Journal of Fatigue* 22 (7) (2000) 569–572. doi:10.1016/S0142-1123(00)00030-X.

- [41] V. Rathod, O. P. Yadav, A. Rathore, R. Jain, Probabilistic modeling of fatigue damage accumulation for reliability prediction, *Journal of Quality and Reliability Engineering* 2011.
- [42] Bureau Veritas, NI638, Guidance for long-term hydro-structure calculations, 2019.
- [43] Det Norske Veritas, DNV-RP-C205, Environmental conditions and environmental loads, 2019.
- [44] A. F. Haselsteiner, R. G. Coe, L. Manuel, P. T. Nguyen, N. Martin, A. Eckert-Gallup, A benchmarking exercise on estimating extreme environmental conditions: methodology and baseline results, in: *International Conference on Offshore Mechanics and Arctic Engineering*, Vol. 58783, American Society of Mechanical Engineers, 2019, p. V003T02A049.
- [45] A. F. Haselsteiner, R. G. Coe, L. Manuel, W. Chai, B. Leira, G. Clarindo, C. G. Soares, Á. Hannesdóttir, N. Dimitrov, A. Sander, et al., A benchmarking exercise for environmental contours, *Ocean Engineering* 236 (2021) 109504.
- [46] E. Mackay, P. Jonathan, Estimation of Environmental Contours Using a Block Resampling Method, Vol. Volume 2A: Structures, Safety, and Reliability of *International Conference on Offshore Mechanics and Arctic Engineering*, 2020. doi:10.1115/OMAE2020-18308.
- [47] G. Lindgren, H. Rootzén, M. Sandsten, *Stationary stochastic processes for scientists and engineers*, Chapman and Hall/CRC, 2013.
- [48] S. O. Rice, Mathematical analysis of random noise, *The Bell System Technical Journal* 23 (3) (1944) 282–332. doi:10.1002/j.1538-7305.1944.tb00874.x.
- [49] S. O. Rice, Mathematical analysis of random noise, *The Bell System Technical Journal* 24 (1) (1945) 46–156. doi:10.1002/j.1538-7305.1945.tb00453.x.
- [50] E. Mackay, G. de Hauteclocque, E. Vanem, P. Jonathan, The effect of serial correlation in environmental conditions on estimates of extreme events, *Ocean Engineering* 242 (2021) 110092.
- [51] R. Hascoët, Level-crossing distributions of kinematic variables in multidirectional second-order ocean waves, *Ocean Engineering* 265 (2022) 112585. doi:10.1016/j.oceaneng.2022.112585.
- [52] F. Pierella, O. Lindberg, H. Bredmose, H. B. Bingham, R. W. Read, A. P. Engsig-Karup, The DeRisk database: Extreme design waves for offshore wind turbines, *Marine Structures* 80 (2021) 103046. doi:10.1016/j.marstruc.2021.103046.
- [53] C. E. Stringari, M. Prevosto, J.-F. Filipot, F. Leckler, P. V. Guimarães, A new probabilistic wave breaking model for dominant wind-sea waves based on the gaussian field theory, *Journal of Geophysical Research: Oceans* 126 (4) (2021) e2020JC016943.
- [54] J. E. Heffernan, J. A. Tawn, A conditional approach for multivariate extreme values (with discussion), *Journal of the Royal Statistical Society: Series B (Statistical Methodology)* 66 (3) (2004) 497–546.
- [55] K. Hasselmann, T. Barnett, E. Bouws, et al., Measurements of wind-wave growth and swell decay during the joint north sea wave project (JONSWAP), *Deutsches Hydrographisches Institut, Hamburg* (1973) 1–95.